Bicho *et al. Molecular Medicine* (2026) 32:68
https://doi.org/10.1186/s10020-026-01456-x

Molecular Medicine

RESEARCH Open Access

# CD5L insufficiency exacerbates skeletal joint damage in rheumatoid arthritis

Diana Bicho[1,2], Malin C. Erlandsson[3,4], David Svensson[3], Emma Comas[1,2], Maria Carolina Silva[1], Venkataragavan Chandrasekaran[3], Victoria M. E. Lundgren[3], Rita F. Santos[1,2,5], Liliana Oliveira[1,2], Maria I. Bokarewa[3,4†] and Alexandre M. Carmo[1,2*†]

## Abstract

**Background and hypothesis** CD5L is a glycoprotein induced during inflammation and makes a life-saving contribution in infection and sepsis. Here, we explored the immunomodulatory effect of CD5L in rheumatoid arthritis (RA). We hypothesized that CD5L availability associates with systemic inflammatory activation during arthritis and stratifies monocyte programs linked to joint structural damage.

**Methods** Using an experimental RA model, we assessed disease development and severity in wild-type and CD5L-deficient mice and characterized circulating immune cell populations and inflammatory mediators. In parallel, human RA mononuclear cells were conditioned with CD5L and analyzed phenotypically and transcriptionally, including CD5L-dependent transcriptome profiling of $CD14^+$ cells and assessment of synovial tissue. Targeted pathway perturbations (HDAC inhibition, Lyn activation, Fcγ receptor engagement) were performed, followed by flow-cytometric phenotyping. These findings were integrated with clinical radiographic scoring and transcriptomic analyses in RA patient material.

**Results** We observed an early surge of CD5L expression in wild-type mice and a higher incidence and increased severity of arthritis in CD5L-deficient mice. CD5L deficiency was associated with enhanced systemic inflammation, expansion of $CD11b^+$ mononuclear cells, and elevated IL-1β, IL-17, and IFN-γ, particularly at the pre-clinical stage of arthritis. In human RA, CD5L-conditioned mononuclear cells, as well as endogenous CD5L production, were associated with reduced CD11b expression, increased IL-10 and PD-L1 production, and enrichment of non-classical $CD16^+$ monocytes. CD5L-dependent transcriptomic profiling of $CD14^+$ cells revealed an efferocytosis-like signature characterized by upregulation of C1Q subunits, *GAS6*, *AXL*, and *ALOX15B*. It also showed reduced expression of genes involved in cargo processing, coinciding with expansion of IFN-primed non-classical monocyte signatures. These CD5L-linked programs correlated strongly with joint damage accrual. Despite markedly low CD5L levels in the synovium, RA synovial tissue was enriched with *GAS6-AXL*$^+$ non-classical monocyte signatures linked to osteoclast progenitor-associated signatures.

†Maria I. Bokarewa and Alexandre M. Carmo contributed equally to this work.

*Correspondence:
Alexandre M. Carmo
acarmo@i3s.up.pt

Full list of author information is available at the end of the article

**Conclusion** This study identifies CD5L as an immunomodulatory factor in experimental and human RA and shows that CD5L availability is associated with efferocytosis-related and IFN-primed monocyte programs. Across experimental arthritis and RA patient material, these CD5L-linked programs correlate with non-classical monocyte expansion and structural joint damage, supporting a model in which CD5L marks a balance between inflammation resolution and monocyte trafficking linked to joint damage.

## Introduction

CD5 antigen-like (CD5L) is a circulating glycoprotein primarily produced by monocytes and macrophages in the spleen, lymphoid tissues, and bone marrow (Gebe et al. 1997). CD5L is best known for its ability to inhibit hematopoietic cell apoptosis (Miyazaki et al. 1999; Sarrias et al. 2004). Among other immunoregulatory roles, it recognizes and neutralizes pathogen-associated molecular patterns (Sarrias et al. 2005; Martínez et al. 2014), and damage-associated molecular patterns released from dying host cells, facilitating debris clearance and limiting tissue inflammation (Arai et al. 2016; Maehara et al. 2021; Kurokawa et al. 2010).

Circulating CD5L levels are elevated in infectious and inflammatory conditions. Yet whether it acts protectively or pathogenically remains uncertain (Sanchez-Moral et al. 2021). Insights into CD5L function have largely come from studies on CD5L-deficient mice, which reveal diverse outcomes depending on the disease model. In an experimental polymicrobial sepsis model, CD5L-deficient mice show impaired neutrophil recruitment, reduced bacterial control, and higher mortality (Oliveira et al. 2024). However, in the context of *Mycobacterium tuberculosis* infection, CD5L deficiency had no detectable impact on disease outcome, even though CD5L levels rise upon infection (Cardoso et al. 2024). CD5L restrains adaptive immunity by impinging on the pathogenic program of Th17 cells. Its absence shifts Th17 cells toward a more pathogenic phenotype (Wang et al. 2015). Additionally, CD5L deletion is protective in several non-infectious conditions, including bleomycin-induced pulmonary fibrosis (Guo et al. 2023) and acetaminophen-induced acute liver injury (Li et al. 2021).

In human autoimmune inflammation, increased serum levels of CD5L have been reported in atopic dermatitis (Kim et al. 2008), systemic lupus erythematosus (Lai et al. 2018), liver fibrosis (Gangadharan et al. 2007), Alzheimer's disease (Riedel et al. 2018), and Kawasaki disease (Yu et al. 2009). In patients with rheumatoid arthritis (RA), circulating CD5L levels were elevated and correlated with disease severity (Wu et al. 2021), suggesting its relevance in joint inflammation. Although this association identifies CD5L as a potential biomarker of inflammation, its functional contribution to RA pathogenesis remains unexplored.

RA is an inflammatory joint disease with an estimated global prevalence of 0.5–1.0% (Almutairi et al. 2021). Morphologically, it is characterized by inflammation of the joint tissue, synovial hyperplasia, and progressive skeletal damage (Isaacs 2010). Monocytes and macrophages play a pivotal role in RA pathogenesis by driving leukocyte infiltration, maintaining a pro-inflammatory cytokine milieu, and inducing synovial hyperplasia and bone remodeling (Gravallese and Firestein 2023; Saeki and Imai 2023).

In RA, monocytes are recruited from the peripheral blood to synovial tissue and differentiate into joint-resident macrophages. Traditionally, circulating monocytes are classified by surface markers into classical ($CD14^+CD16^-$), intermediate ($CD14^+CD16^+$), and non-classical ($CD14^{low}CD16^+$) subtypes (Murray et al. 2014). Functionally, classical monocytes are highly phagocytic and pro-inflammatory, intermediate monocytes focus on inflammatory cytokine production and contribute to antigen presentation, while non-classical monocytes patrol the endothelium and support tissue repair (Salnikova et al. 2024).

Single-cell analyses of RA synovial tissue refined the identification of distinct macrophage subsets with specialized roles in the disease pathogenesis. One study identified a pro-inflammatory population characterized by high production of IL-6 and TNF and lacking expression of the receptor tyrosine kinase MerTK, a key molecule involved in efferocytosis (Alivernini et al. 2020). In contrast, $CX3CR1^+MerTK^+$ macrophages function as organizers of the immunological barrier and support resolution of inflammation (Culemann et al. 2019; Faas, et al. 2021; Cai et al. 2018). Another study revealed a distinct subset of inflammatory macrophages that promotes fibroblast aggressiveness and invasion through expression of heparin-binding EGF-like growth factor, urokinase receptor, and NR4A family transcription factors (Kuo et al. 2019).

The emergence of macrophage phenotypic states is strongly influenced by epigenetic mechanisms. In RA, an altered balance between histone acetyltransferase (HAT) and histone deacetylase (HDAC) activities leads to global histone hyperacetylation, increasing chromatin accessibility at both inflammatory and regulatory gene loci (Klein et al. 2012; Yang et al. 2022). Reduced HDAC activity contributes to the histone hyperacetylation in macrophages, amplifying NF-κB-driven IL-6 and TNF production (Li et al. 2018; Angiolilli et al. 2017). Conversely, certain HDACs, including SIRT1, can

epigenetically promote IL-10 expression, driving macrophage polarization toward a pro-resolving M2 phenotype (Yang et al. 2022). Thus, histone acetylation acts as a context-dependent regulatory mechanism capable of either sustaining inflammation or facilitating its resolution.

Despite advances in understanding the cellular and epigenetic drivers of RA, the immunomodulatory role of CD5L in disease development remains poorly explored. We hypothesized that CD5L availability is associated with reduced systemic inflammatory activation during arthritis and that variation in CD5L levels in RA patients stratifies monocyte programs linked to joint structural damage. To test this hypothesis within a translational framework, we integrated in vivo observations from *Cd5l*$^{-/-}$ mice in the CIA model with ex vivo experiments in human cells involving recombinant CD5L stimulation and targeted intracellular pathway perturbation, followed by flow cytometry–based phenotyping. We then aligned these findings with clinical and radiographic RA cohorts, bulk transcriptomics of sorted CD14$^{+}$ cells, and validation in single-cell datasets from PBMCs and synovial tissue. Accordingly, the objective of this study was to define and integrate the experimental and clinical associations between CD5L and monocyte inflammatory/resolution programs in RA and to relate these programs to joint structural damage.

## Materials and methods

### Ethics statement

All animal experiments were conducted in strict accordance with the Portuguese (Portaria 1005/92) and European (Directive 2010/63/EU) legislations governing the housing, husbandry, and welfare of laboratory animals. The study protocols were reviewed and approved by the Ethics Committee of the Instituto de Investigação e Inovação em Saúde (i3S), Universidade do Porto, and by the Portuguese National Entity Direção Geral de Alimentação e Veterinária (license references: 022868/2020–12–31 and 009951/2018–05–17).

Human studies received the approval from the Regional Ethical Committee of Gothenburg, Sweden (Cohort 1: Dnr 659–11; Cohort 2: Dnr 2019–03787). The collection of biological material was conducted in accordance with national regulations and the International Conference on Harmonization Good Clinical Practice requirements, based on the Declaration of Helsinki.

### Mice and experimental procedures

CD5L knockout (*Cd5l*$^{-/-}$, hereafter referred to as CD5L-deficient or CD5L$^{-}$) mice on a C57BL/6 J background, generated by CRISPR/Cas9 engineering and previously characterized in our laboratory (Oliveira et al. 2024), were maintained under specific pathogen-free conditions at the i3S animal facility (Porto, Portugal). Wild-type (*Cd5l*$^{+/+}$, hereafter WT) littermates were used as controls. Peripheral blood analyses revealed no major differences in leukocyte counts or subset distribution between WT and CD5L$^{-}$ mice.

All experiments were performed using 8–12-week-old male mice bred in-house. Male mice were selected due to their higher susceptibility to CIA. Animals were housed at 21 ± 2 °C under a 12-h light/dark cycle, with ad libitum access to food and water, in an AAALAC-accredited facility.

### Induction and evaluation of collagen-induced arthritis (CIA)

CIA was induced as previously described (Nogueira et al. 2015), replacing bovine with chicken type II collagen (CII) (Chondrex, cat. no. 20012, Woodinville, WA, USA). On day 0, mice were immunized subcutaneously at the base of the tail with 0.2 mg of chicken CII emulsified in an equal volume of complete Freund's adjuvant (CFA, Chondrex, cat. no. 7023; 0.5 mg/mouse; total volume 200 µl). On day 21, mice received a booster injection of CII in incomplete Freund's adjuvant (Sigma-Aldrich, cat. no. F5506, St. Louis, MO, USA).

#### *Arthritis evaluation*

Arthritis severity was evaluated in all four paws using a blinded scoring system by a trained observer. Each paw was scored for swelling and erythema: 0 = normal, 1 = mild swelling/erythema, 2 = pronounced swelling, 3 = deformity, 4 = ankylosis. The maximum score achieved for each joint (ankle, tarsus, carpus, toes and finger) was 4, so the maximum arthritis score for a single mouse on a given day could reach 40. Mice were evaluated two to three times per week, and body weight was recorded weekly.

#### *Blood collection*

Blood samples were drawn using the facial vein. For that, animals were anesthetized with inhaled isoflurane administered with 1 bar of oxygen at 5% concentration. Blood was collected at the different time points using a 23G needle followed by aspiration into a 75 µl heparinized microhematocrit tube (Fisher Scientific, Hampton, NH, USA), and stored in Eppendorf tubes for 30 min at RT. Subsequently, the serum was separated from the clotted blood by centrifugation at 9,000 × *g* at 4 °C for 10 min and stored at −20 °C until further use.

#### *Immunophenotyping of mouse leukocytes*

Blood was treated with red blood cell lysis buffer (0.01 M Tris, 0.15 M $NH_4Cl$, pH 7.2) at RT for 5 min. Subsequently, the cells were centrifuged at 300 × *g* for 5 min at 4 °C, washed in 50 µl FACS buffer [0.2% (w/v) BSA + 0.1% (w/v) $NaN_3$ in PBS] and centrifuged again and blocked

using FcR-block [TruStain FcX™ (anti-mouse CD16/32), BioLegend, San Diego, CA, USA] for 15 min on ice. After a new centrifugation, the cells were incubated for 30 min with the following antibodies (all BioLegend, San Diego, CA, USA unless otherwise stated): CD3 APC-Cy7 (17A2), CD19 APC (6D5), NK1.1 FITC (PK136), CD11b PE (M1/70), F4/80 APC-Cy7 (BM8), Ly6C FiTC (HK1.4), Ly6G PB (1A8), and Siglec-F Alexa Fluor® 647 (E50-2440, BD Biosciences, Franklin Lakes, NJ, USA). After washes, cells were resuspended in FACS buffer, filtered using a 0.2 µm cell strainer and data were acquired on a three-laser BD FACSCanto II (Becton Dickinson). Data analysis was performed in FlowJo v10.10.0 (BD Biosciences).

The phenotyping gating strategy is shown in Fig. S1. Cells were identified as T cells ($CD3^+$), B cells ($CD19^+$), NK cells ($NK1.1^+CD3^-$), eosinophils ($SSC^{hi}Siglec\text{-}F^+CD11b^+$), neutrophils ($Siglec\text{-}F^-Ly6G^+CD11b^+$), monocytes ($Siglec\text{-}F^-Ly6G^-F4/80^+CD11b^+$), classical/inflammatory monocytes ($Siglec\text{-}F^-Ly6G^-F4/80^+CD11b^+Ly6C^+$), and patrolling/non-classical monocytes ($Siglec\text{-}F^-Ly6G^-F4/80^+ CD11b^+ Ly6C^-$).

#### *Quantification of soluble factors*

Bone resorption markers RANKL and cross-linked C-telopeptide of type I collagen (CTX-I) were measured in the sera of WT and $CD5L^-$ mice using the Mouse RANKL ELISA development Kit (#900-K233K, Peprotech) and Mouse C-telopeptide of type I collagen, CTX-I ELISA Kit (#MBS164705, MybioSource), respectively. Cytokine levels in the serum of WT and $CD5L^-$ mice were measured using ELISA Max™ Deluxe Sets (BioLegend) for IL-17A (#432,504), IL-1β (#437,004), IL-6 (#431,304), and IFN-γ (#430,804). CD5L serum levels were quantified using the Mouse CD5L ELISA Pair Set (Sino Biological, SEK50020). Anti-CII antibodies were quantified by in-house ELISA using microtiter plates (Nunc MaxiSorp™, 44–2404-21, Thermo Fisher Scientific) coated overnight at 4 °C with 5 µg/ml CII dissolved in coating buffer (0.05 M Tris, 0.2 M NaCl, pH 7.4). The plates were washed with 0.05% (v/v) Tween 20 in PBS and blocked with 5% foetal bovine serum in PBS for 1 h. The test serum was serially diluted and added to the collagen-coated plate for 2 h. Total bound IgG was detected with goat anti-mouse IgG-HRP (Poly4053, BioLegend), followed by substrate solution (SIGMAFAST™ OPD, P9187, Sigma-Aldrich). Reactions were stopped with 3 N $H_2SO_4$ and the optical density was measured at 492 nm using a µQuant™ Microplate Reader (BioTek Instruments). Results were plotted using GraphPad Prism, with 1/serum dilution on the x-axis (log scale) and optical density (OD) on the y-axis (linear scale). A pooled serum sample from CII-immunized mice was serially diluted and included on each plate as a standard to ensure inter-plate reproducibility.

**Table 1** Clinical characteristics of the patients with rheumatoid arthritis

| **All female** | **Cohort 1 + 2** ***n*** **= 80** | **Cohort 2 (RNAseq)** ***n*** **= 35** |
|---|---|---|
| Age, y mean (min–max) | 60.9 (29–76) | 64.9 (46–76) |
| DD, y mean (min–max) | 14.7 (1–45) | 12.8 (1–45) |
| AB-positive | 69 (86.2) | 28 (80%) |
| RF-positive | 66 (82.5) | 26 (74.3%) |
| ACPA-positive | 62 (77.5) | 18 (51.4%) |
| DAS28, mean (min–max) | 3.17 (1.07–5.77) | 2.87 (1.07–5.77) |
| Total Sharp-vdH score, mean (min–max) | 52.0 (0.299) | 44.8 (8–58) |
| Treatment | | |
| MTX | 64 (80%) | 24 (68.6%) |
| TNF-inhibitors | 51 (63.6%) | 10 (28.6%) |
| Other DMARDs | 5 (6.2%) | 2 (5.7%) |

*DD* Disease duration, *AB* Antibodies, *RF* Rheumatoid factor, *ACPA* Antibodies to citrullinated peptides, *DAS28* Disease activity score by 28 joints, *Sharp-vdH* Sharp van der Heide, *MTX* Methotrexate, *TNF* Tumor necrosis factor, *DMARDs* Disease modifying anti-rheumatic drugs

### Human samples

#### *Cohorts and clinical data*

The study included 80 female patients with established RA (mean age 60 ± 12 years; mean disease duration 14.7 years) who were attending the Rheumatology Clinic at Sahlgrenska University Hospital, Gothenburg. Cohort 1 was collected during 2012–2013, cohort 2 was collected during 2019. Demographic and clinical characteristics of the patient cohorts are summarized in Table 1. In 2016, CD5L was measured in the serum of 40 patients with RA, 11 healthy controls, and an additional 5 paired samples of blood and synovial fluid. In 2024, we measured CD5L levels in the serum of 35 RA patients and in supernatants of $CD14^+$ cell cultures isolated from the same individuals.

Disease-modifying antirheumatic drugs were used by 73 of 80 patients, including methotrexate (MTX) in 64 patients. Five patients received other agents (azathioprine, $n = 3$; chlorambucil, $n = 1$; leflunomide, $n = 1$). TNF inhibitors were administered to 51 patients, all in combination with MTX or other disease-modifying agents. All patients and healthy controls provided written informed consent prior to participation in study-related procedures.

#### *Sample collection and processing*

Blood samples were collected in sterile vacuum tubes containing sodium citrate (0.129 mol/l, pH 7.4) for plasma, and in additive-free tubes for serum**.** Samples were then placed on ice until centrifugation ($1600 \times g$, 4 °C, 15 min). Serum and plasma supernatants were aliquoted into RNAse/DNAse-free tubes and stored at −80 °C until further use.

Synovial fluid samples were obtained by arthrocentesis of knee joints prior to routine corticosteroid injection. SF was aspirated aseptically and transferred into tubes containing sodium citrate, aliquoted, and stored at −80 °C until analysis. All samples were coded and analyzed by investigators blinded to the clinical and radiological data.

#### *Clinical data collection*

A standard protocol for evaluation of joints was used considering the swelling, tenderness, limited motion or deformity of each joint (Pincus et al. 1999). Disease activity was measured with the disease activity score in 28 joints (DAS28), including 10 metacarpal phalangeal and 10 proximal interphalangeal joints of the hands, 2 shoulders, 2 elbows, 2 wrists, and 2 knees. The DAS28 scores were calculated based on the number of tender and swollen joints, and erythrocyte sedimentation rate (ESR) (Aletaha et al. 2006).

#### *Radiographic evaluation*

The degree of radiographic joint damage was calculated from posterior-anterior radiographs of the hands and feet using the Sharp method modified by van der Heijde (vdH-Sharp) (Heijde et al. 1992). The vdH-Sharp score was presented as a total score (range: 0–448), including an erosion score (0–280), and a joint space narrowing score (0–168). The total vdH-Sharp > 50 characterized severe radiographic damage.

### Serological measurements

CD5L levels in serum and synovial fluid were quantified using the human CD5L ELISA kit (ab213760; Abcam, Cambridge, UK); detection limit, 10 pg/ml. CD5L levels from serum from RNAseq samples and supernatants from PBMC and $CD14^+$ cell cultures were quantified using the human CD5L ELISA kit (EH94RB, Invitrogen, Waltham, MA, USA); detection limit, 0.3 pg/ml.

Cartilage oligomeric matrix protein (COMP) levels were measured by an ELISA kit (Anamar, Lund, Sweden) in samples diluted 1:10; detection limit, 0.9 IU/ml. C-telopeptide cross-link type I collagen (CTX-I) was measured by an ELISA (IDS Serum CrossLaps, Immunodiagnostic Systems, Boldon, UK) in undiluted samples; detection limit, 0.11 ng/ml. Matrix metalloproteinase 3 (MMP-3) levels were measured by an ELISA using a pair of matched antibodies (DY513, R&D Systems, Minneapolis, MN, USA) in samples diluted 1:100; detection limit, 3 ng/ml.

Cytokine levels were determined by a sandwich ELISA: IL-10 (DY217B, R&D Systems; detection limit, 3 pg/ml), IFN-γ (DY285B, R&D Systems; detection limit, 5 pg/ml), and PD-L1 (DY156, R&D Systems; detection limit, 0.5 pg/ml).

In cohort 1, IGF-1 levels were measured by an ELISA using a pair of matched antibodies (DY291, R&D Systems) in samples diluted 1:25; detection limit, 1 ng/ml. In cohort 2, IGF-1 levels were analyzed by photometry on the Cobas 8000 system (Roche Diagnostics, Basel, Switzerland). All detection limits are reported according to the manufacturers' instructions.

### Isolation and stimulation of human $CD14^+$ cells

Human peripheral blood mononuclear cells (PBMCs) were isolated from heparinized venous peripheral blood by density gradient separation on Lymphoprep (Axis-Shield PoC AS, Dundee, Scotland). PBMC cultures ($1 \times 10^6$ cells/ml) were propagated in RPMI medium (Gibco, Waltham, MA, USA) containing 50 µM β-mercaptoethanol (Gibco), 2 mM GlutaMAX (Gibco), 50 µg/ml gentamicin (Sanofi-Aventis, Paris, France), and 5% fetal bovine serum (Sigma-Aldrich) at 37 °C in a humidified 5% $CO_2$ atmosphere.

Cells were stimulated with concanavalin A (ConA, 0.625 µg/ml; Sigma-Aldrich) and lipopolysaccharide (LPS, serotype O55:B5, 5 µg/ml; Sigma-Aldrich) for 48 h. After 24 h, some cultures were supplemented with HDAC inhibitor valproate (50 µg/ml; Ergenyl, Sanofi, Paris, France), human recombinant CD5L (1 µg/ml (INVIGATE GmbH, Jena, Germany), human IgG (4 µg/ml; Kiovig, Takeda, Tokyo, Japan), or a combination of CD5L with human IgG, as indicated. The synthetic Lyn activator talimogene (1 and 10 µg/ml; Selleckchem, Houston, USA) was also used.

$CD14^+$ cells were isolated from fresh PBMC cultures by positive selection (kit #17,858; StemCell Technologies, Vancouver, Canada) and propagated in the enriched RPMI medium described above at a concentration of $1.25 \times 10^6$ cells/ml. For RNAseq and qPCR, cells were stimulated with LPS (5 µg/ml) for 2 h.

At the end of incubation, supernatants were collected for cytokine measurement, and cells were analyzed by flow cytometry. Adherent cells were detached by incubation with 1 mM ice-cold EDTA for 15 min, followed by gentle mechanical scraping. Adherent and non-adherent cells were pooled for subsequent analysis.

### Flow cytometry

Cells were resuspended in PBS containing 2% fetal bovine serum, 0.1% $NaN_3$ and 1 mM EDTA (FACS buffer). Non-specific binding was blocked with human γ-globulin (100 µg/ml, Kiovig, Takeda). Cells were then stained with monoclonal mouse anti-human antibodies: CD4-Brilliant Violet 510 (Clone SK3, Beckton Dickinson (BD), Franklin Lakes, NJ, USA), CD14-PE (Clone M5E2, BD), CD16-FITC (Clone ME5E2, BD), CD29-APC (Clone MAR4, BD), CD11b-Pacific Blue (Clone CRF44,

BD), CD45-PerCP (Clone 2D1, BD). All antibodies were diluted in FACS buffer to optimal concentrations.

Cells (100,000 events/sample) were acquired in a FACS-Lyric (Beckton Dickinson) and analyzed with FlowJo v10.10 software (Beckton Dickinson). Cell populations were gated using fluorochrome minus one (FMO) staining controls. The analysis was done within the $CD4^{-}CD11b^{+}$ gate divided into $CD14^{+}CD16^{-}$ (classical monocytes); $CD14^{+}CD16^{+}$ (intermediate monocytes); and $CD14^{low}CD16^{+}$ (non-classical monocytes). Data are presented as the percentage of $CD4^{-}CD11b^{+}$ cells or as mean fluorescence intensity (MFI) in positive cells.

#### Transcriptome sequencing (RNA-seq) and analysis

Total RNA from $CD14^{+}$ cells was isolated using the Norgen Total RNA Kit (17,200, Norgen Biotek, Ontario, Canada). RNA quality was assessed using the RNA 6000 Pico Kit on an Agilent 2100 Bioanalyzer (Agilent Technologies, Santa Clara, CA, USA). High-throughput sequencing was performed by RNA-seq (HiSeq 2000, Illumina) at the core facility for Bioinformatics and Expression Analysis, Karolinska Institutet (Huddinge, Sweden). Raw sequence data were generated as BCL files and converted to FASTQ format using Illumina's bcl2fastq software.

Analysis was performed using the core Bioconductor packages in R-studio v. 4.4.1. Mapping of transcripts was done using Genome UCSC annotation set for hg38 human genome assembly. Using the normalized expression data in $CD14^{+}$ cells of 35 RA patients, the 'rank metric score' was used to rank the protein coding genes. For each gene transcript, the rank metric score was calculated as difference of the mean expression scaled by the standard deviation and identified the genes acting as reliable markers of this gene set. The genes with the rank metric score above 0.200 were used in the linear regression analysis of z-standardized serum CD5L levels and of CD5L levels in supernatants of $CD14^{+}$ cells to the transcriptome.

Using the design formula ~ log_CD5L_scaled in the DESeq2 pipeline, we identified protein-coding genes with a base mean expression ≥ 10 that showed a significant change ($|\log_2 FC| > 0$, nominal $p \leq 0.05$) per unit increase in serum CD5L levels. These genes were subsequently analyzed for enriched biological pathways using Gene Set Enrichment Analysis (GSEA) via the online tool provided by the Broad Institute (in collaboration with UC San Diego, USA).

#### *Analysis of the single-cell transcriptome in myeloid cells of synovial tissue*

To analyze CD5L-dependent gene signatures, we used the single-cell transcriptome dataset of synovial tissue of RA patients (Zhang et al. 2023). The log-normalized mRNA matrix was used to create the Seurat object and subset to the myeloid cell cluster ($n = 76{,}181$ cells). Within this subset, the joint density of gene expression for different gene signatures was calculated and visualized using the do_NebulosaPlot function from the SCpubr package (Blanco-Carmona 2022). CD5L expression was visualized by dot plots using the Dotplot_scCustom function from the scCustomize package (Marsh and scCustomize 2021).

#### Data availability

Transcriptome sequencing data of $CD14^{+}$ cells from 35 RA patients is deposited in NCBI GEO with accession GSE282517. Single-cell transcriptomic data of RA synovial tissue are publicly available on Synapse (https://doi.org/10.7303/syn52297840).

#### Statistical analysis

Since different methods were used for the measurement of serum CD5L, and IGF-1 in the patient cohorts 1 and 2, the measurements were individually z-transformed and then pooled for further analysis.

Statistical analyses were performed using GraphPad Prism (version 10.1.1; GraphPad Software LLC, San Diego, CA, USA). The specific statistical tests applied are detailed in each figure legend, and relevant comparisons are shown in each graph. Differences were considered statistically significant at a $P$-value ≤ 0.05 (95% confidence level). Significance levels are indicated as follows: $^{*}p < 0.05$, $^{**}p < 0.01$, $^{***}p < 0.001$, $^{****}p < 0.0001$.

## Results

#### Experimental CIA in *Cd5l*$^{-/-}$ mice: CD5L delays arthritis development

CIA was induced in WT (n = 36) and $CD5L^{-}$ (n = 39) mice by intradermal immunization with chicken CII across five independent experiments. Disease incidence, onset, and severity were monitored over 56 days. In $CD5L^{-}$ mice, arthritis was first detected by joint swelling on day 23, just two days after the booster CII injection on day 21. By comparison, CIA appeared later in WT controls. $CD5L^{-}$ mice developed CIA more frequently than WT mice (maximum incidence 35% vs. 22%, $p = 0.126$), with the most pronounced differences during early disease (day 23, $p = 0.032$, and day 28, $p = 0.066$) (Table 2 and Fig. 1A). Arthritis onset was also earlier in $CD5L^{-}$ mice, which exhibited a mean onset of 30.4 ± 7.5 days compared with 35.6 ± 7.5 days in WT controls ($p = 0.08$; WT: AUC = 6.958, SE = 4.962, 95% CI 0.00–16.68; $CD5L^{-}$: AUC = 14.48, SE = 10.13, 95% CI 0.00–34.34).

Throughout the course of CIA, $CD5L^{-}$ mice tended to develop more severe clinical disease, as indicated by both the number of swollen joints and the magnitude of swelling, although these differences did not reach statistical significance (Fig. 1B). Weight loss, a robust indicator of systemic inflammation in CIA, differed between WT and

**Table 2** Incidence of CIA in WT and CD5L-mice

| Days post immunization | | Cases | % Incidence | 95% CI* | $p^{\#}$ |
|---|---|---|---|---|---|
| 1 | WT | 0/36 | 0 | –- | –- |
| | CD5L$^-$ | 0/39 | 0 | | |
| 5 | WT | 0/36 | 0 | –- | –- |
| | CD5L$^-$ | 0/39 | 0 | | |
| 15 | WT | 0/36 | 0 | –- | –- |
| | CD5L$^-$ | 0/39 | 0 | | |
| 23 | WT | 0/36 | 0 | 1.12–24.5 | 0.032 |
| | CD5L$^-$ | 5/39 | 12.8 | | |
| 28 | WT | 4/36 | 11.1 | 1.26–40.6 | 0.066 |
| | CD5L$^-$ | 12/39 | 30.8 | | |
| 30 | WT | 5/36 | 13.9 | 4.69–38.5 | 0.125 |
| | CD5L$^-$ | 12/39 | 30.8 | | |
| 35 | WT | 6/36 | 16.7 | 8.09–36.3 | 0.213 |
| | CD5L$^-$ | 12/39 | 30.8 | | |
| 37 | WT | 7/36 | 19.4 | 7.52–40.4 | 0.179 |
| | CD5L$^-$ | 14/39 | 35.9 | | |
| 41 | WT | 7/36 | 19.4 | 11.5–34.1 | 0.330 |
| | CD5L$^-$ | 12/39 | 30.8 | | |
| 44 | WT | 7/36 | 19.4 | 9.50–37.3 | 0.245 |
| | CD5L$^-$ | 13/39 | 33.3 | | |
| 47 | WT | 8/36 | 22.2 | 18.8–25.6 | 0.763 |
| | CD5L$^-$ | 10/39 | 25.6 | | |
| 51 | WT | 8/36 | 22.2 | 16.8–28.8 | 0.607 |
| | CD5L$^-$ | 11/39 | 28.2 | | |
| 56 | WT | 7/36 | 19.4 | 13.4–31.0 | 0.440 |
| | CD5L$^-$ | 11/39 | 28.2 | | |

Data of experiments represented in Fig. 1a. All mice were male between 8 and 12 weeks of age

*95% Confidence interval of the Incidence rate difference, according with the "Test-based method" in Sahai H., Khurshid A. (1996)

#*P*-value after comparison between the rates of incidence of WT and CD5L-animals obtained using the Chi2-statistic

CD5L$^-$ mice that developed arthritis (Fig. 1C). Fig. S2A shows the mouse weight at day 0 and subsequent weight changes in CIA experiments. At day 37, at the peak of CIA severity, the weight loss strongly correlated with arthritis scores in WT mice, whereas this association was absent in CD5L$^-$ mice (Fig. 1D). Histological examination of affected joints revealed dense inflammatory infiltrates, evidence of joint effusion, and, in some cases, focal loss of bone surface integrity (Fig. S2B).

### Early serum CD5L changes and inflammatory cell dynamics during CIA

To characterize the role of CD5L in CIA, we first measured serum CD5L levels in WT mice ($n = 16$, 1 developing arthritis). CD5L levels increased from approximately 0.81 µg/ml at day 0 to a mean of 2.65 µg/ml at day 14 ($p = 0.0040$) (Fig. 2A), then declined progressively and did not rise after the booster immunization. A modest increase was observed at day 56, without altering the overall pattern. No clinical arthritis was detected during the early CD5L surge, and when levels returned to baseline.

In parallel, we compared WT and CD5L$^-$ mice to evaluate immune cell dynamics and systemic inflammation ($n = 6$; 1 WT and 3 CD5L$^-$ mice developed arthritis). CD5L$^-$ mice displayed the increased frequency of circulating monocytes (Siglec-F$^-$Ly6G$^-$F4/80$^+$CD11b$^+$), affecting both classical inflammatory (Ly6C$^+$) and non-classical patrolling (Ly6C$^-$) subsets during the first week after CII immunization, and these elevations persisted over time (Fig. 2B). In contrast, neutrophils (Fig. S3A), and CD11b$^+$ myeloid cells (Fig. 2B) were initially enriched in CD5L$^-$ mice but were diminished and levelled off after day 14. Thus, while the elevation in total CD11b$^+$ cells was transient, the enrichment in monocytes sustained throughout the disease course. The peripheral blood populations of T and NK cells remained unaltered during CIA, while B cells and eosinophils were transiently decreased on day 14, with no differences between CD5L$^-$ and WT mice (Fig. S3A). These percentages represent relative frequencies within total circulating leukocytes and therefore reflect shifts in overall leukocyte composition rather than absolute depletion of specific cell types.

Serum cytokine analyses revealed that CD5L$^-$ mice had a pre-existing inflammatory background, with elevated IL-17A and IFN-γ at day 0 (Fig. 2C). Following CII immunization, IL-17A levels continued to rise, accompanied by IL-1β and IL-6. IL-1β levels correlated with the expansion of inflammatory monocytes. In contrast, WT mice did not exhibit a comparable cytokine surge. The marked

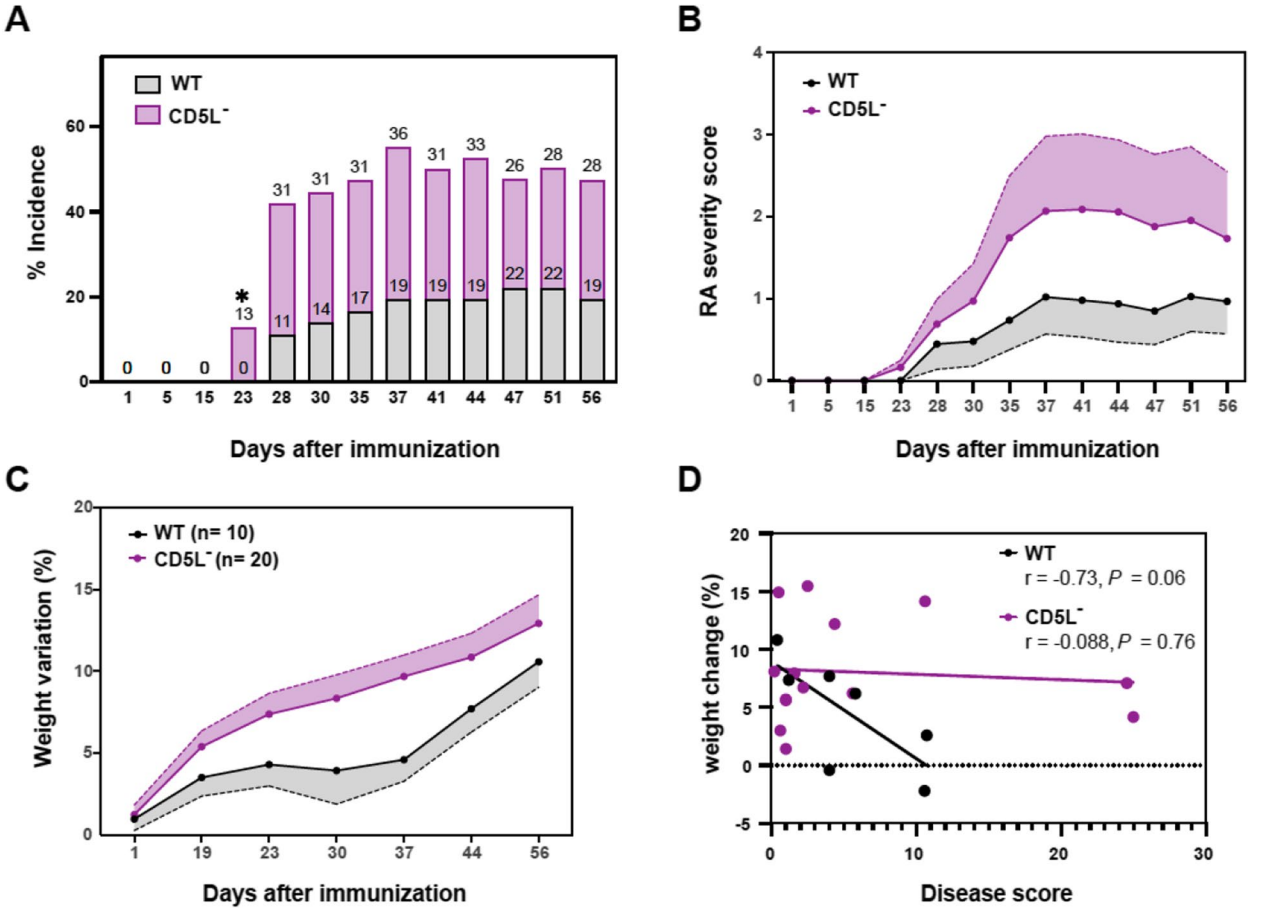


**Fig. 1** Incidence and severity of collagen-induced arthritis in WT and CD5L⁻ mice. **A** Column plot of arthritis incidence from five independent experiments. WT ($n = 36$) and CD5L⁻ ($n = 39$) mice. $p$-values were obtained using the $\chi^2$ test (see Table 2). $p < 0.05$. **B** Line plot of mean clinical arthritis severity. The shaded area represents SEM. **C** Line plot of mean change in body weight. **D** Dot plot of weight change in relation to disease severity score. Lines represent Pearson correlations in WT and CD5L⁻ mice

rise in CD5L in WT mice (Fig. 2A) is consistent with the absence of early pro-inflammatory cytokine release. Anti-CII antibody levels increased sharply after the booster at day 31 and continued rising throughout CIA, with no significant differences between genotypes (Fig. S3B).

To assess the impact of CD5L deficiency on bone remodeling, we measured serum markers of bone resorption. CD5L⁻ mice showed elevated CTX-I levels, whereas serum RANKL remained similar to WT mice (Fig. 2D). To explore mechanisms linking inflammation and osteoclast activity, we analyzed splenic expression of *Gas6*, *Axl*, *Alox8*, and *Vsig4*, genes involved in anti-inflammatory signaling and regulation of monocyte/macrophage activity. In CD5L⁻ mice, *Vsig4* expression was significantly increased, suggesting a compensatory response to persistent immune activation. In contrast, *Axl*, *Gas6*, and *Alox8* expression remained unchanged (Fig. 2E).

Taken together, the early rise in serum CD5L in WT mice appeared to confer protection during CIA, whereas CD5L⁻ mice had elevated baseline levels of serum IL-17 and IFN-γ, leading to sustained inflammatory monocyte expansion and more severe arthritis.

### Ex vivo modulation of human mononuclear cells: CD5L promotes an anti-inflammatory phenotype in human monocytes

To provide experimental evidence linking CD5L to the regulation of monocyte phenotypes, PBMCs ($n = 8$) were activated with LPS and ConA and subsequently exposed to recombinant CD5L (rCD5L; 1 µg/ml), or rCD5L + IgG, for 24 h before flow cytometric analysis. Gating on CD4⁻ CD11b⁺ monocytes, we found that CD5L treatment reduced surface expression of the αM-integrin CD11b, as measured by MFI ($p = 0.031$). Furthermore, the combined rCD5L + IgG condition decreased the expression of β1-integrin (CD29) on CD14⁺ monocytes ($p = 0.031$), indicating a regulatory effect that may further limit monocyte migratory and tissue-infiltrative capacity (Fig. 3A).

Analysis of the classical, intermediate, and non-classical monocyte subsets revealed no significant effect of rCD5L stimulation (Fig. S4A, S4B). However, among

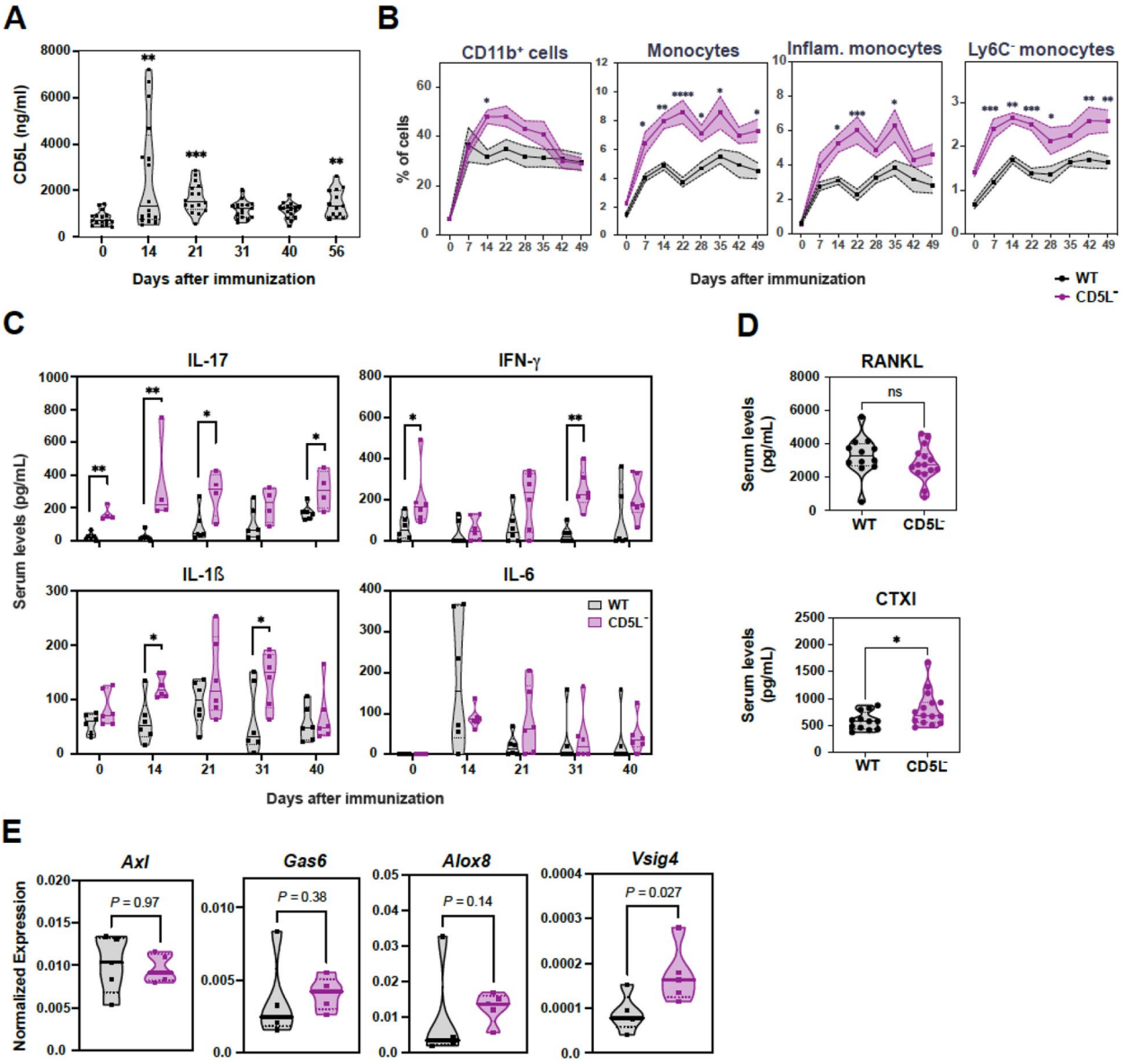


**Fig. 2** Immune profile of WT and CD5L⁻ mice during CIA. **A** Serum CD5L levels measured in WT mice after immunization. *p*-values were obtained using the Kruskal–Wallis test with Dunn's multiple comparisons. **B** Frequencies of blood leukocyte subsets in WT ($n = 10$) and CD5L⁻ ($n = 10$) mice. Leukocytes were phenotyped by flow cytometry: CD11b⁺ cells, monocytes (Siglec-F⁻Ly6G⁻F4/80⁺CD11b⁺); inflammatory monocytes (Siglec-F⁻Ly6G⁻F4/80⁺CD11b⁺Ly6C⁺); and Ly6C⁻ monocytes (Siglec-F⁻Ly6G⁻F4/80⁺CD11b⁺Ly6C⁻). Shaded area indicates mean and SEM of total leukocyte frequency. *p*-values were calculated using Šídák's multiple-comparisons test. **C** Serum cytokine levels in WT ($n = 6$) and CD5L⁻ ($n = 6$) mice. *p*-values were calculated using the Mann–Whitney test. **D** Serum RANKL and cross-linked C-telopeptide of type I collagen (CTX-I) levels on day 56 after immunization. *p*-values were obtained using an unpaired *t*-test with Welch's correction. **E** Splenic gene expression in non-immunized WT ($n = 5$) and CD5L⁻ ($n = 5$) mice, measured by RT-qPCR and normalized to *Actb* (β-actin). *p*-values were calculated using a two-tailed unpaired *t*-test with Welch's correction

the intermediate and non-classical monocytes, rCD5L increased the expression intensity of CD16/FCGRIIIA, shifting the balance toward the non-classical monocytes (Fig. 3B). Surface expression of the TLR4 receptor CD14 remained unaffected by rCD5L stimulation.

Measurement of cytokine production in supernatants from rCD5L-stimulated cells revealed a significant increase in IL-10 ($p = 0.016$), GAS6 ($p = 0.016$), and PD-L1 (rCD5L + IgG, $p = 0.008$) protein levels, while IFN-γ production was unchanged (Fig. 3C). IL-10 levels positively correlated with CD16 MFI (Spearman $\rho = 0.511$, $p = 0.018$) and negatively correlated with CD11b MFI on CD4⁻CD11b⁺ monocytes ($\rho = -0.616$, $p = 0.003$) and on non-classical CD14$^{low}$CD16⁺ monocytes ($\rho = -0.729$, $p = 0.0002$).

Taken together, these findings indicate that rCD5L exerts anti-inflammatory effects by suppressing integrin expression while promoting IL-10 and PD-L1 production,

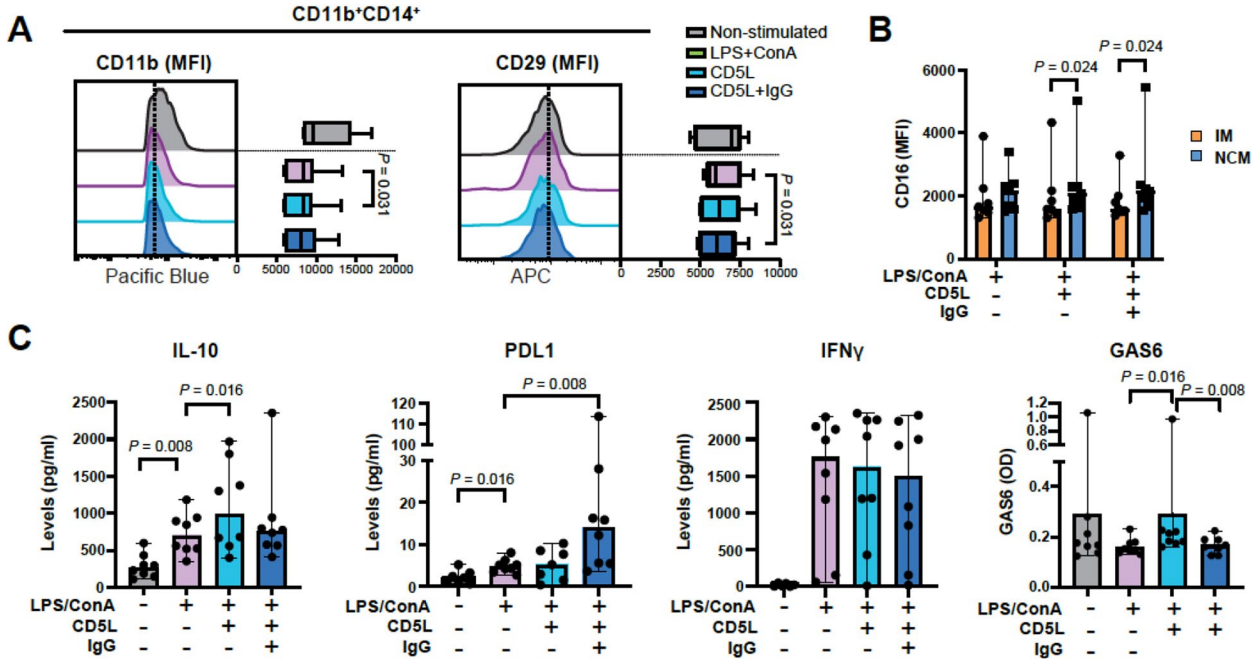


**Fig. 3** CD5L induces an anti-inflammatory phenotype in human monocytes. **A** Representative flow cytometry histograms showing CD11b and CD29 expression in human CD11b⁺CD14⁺CD4⁻ cells stimulated as indicated. Mean fluorescence intensity (MFI) of CD11b and CD29 is shown for $n = 8$ donors. *p*-values were calculated using the paired Wilcoxon test. **B** CD16 expression on intermediate (IM; CD14⁺CD16⁺) and non-classical (NCM; CD14$^{low}$CD16⁺) monocyte subsets. **C** Protein levels of IL-10, PD-L1, IFN-γ, and GAS6 measured in culture supernatants. * $p < 0.05$; ** $p < 0.01$; *** $p < 0.001$

a profile associated with increased proportions of non-classical monocytes.

### Histone acetylation-dependent production of CD5L by human PBMCs

To examine CD5L production by human monocytes, we stimulated freshly prepared PBMC cultures ($n = 20$) with LPS + ConA and subsequently stimulated them with Fcγ-receptor ligand IgG, class I HDAC inhibitor (HDACi, valproate), and Lyn agonist (LynA, talimidone), to induce an anti-inflammatory response. We found that CD5L protein levels were not increased significantly after 48 h of stimulation with LPS + ConA, while addition of HDACi to LPS + ConA-stimulated PBMCs demonstrated a significant rise in CD5L production ($p = 0.0001$) (Fig. 4A). CD5L production remained unchanged/low after cell stimulation using LynA (Fig. S4C). The HDACi-induced increase of CD5L production coincided with a significant increase of IL-10 production ($p = 0.011$) and a decrease of IFN-γ ($p = 0.002$), GAS6 ($p = 0.067$), and PD-L1 ($p = 0.008$) (Fig. 4A). LynA affected neither CD5L nor IFN-γ production by PBMC cultures stimulated with HDACi (Fig. S4C, S4D). Correlation analyses showed that IFN-γ production had an inverse association with CD5L ($\rho = -0.494$, $p = 0.004$), IL-10 ($\rho = -0.541$, $p = 0.0014$) and CD16 expression ($\rho = -0.469$, $p = 0.010$. Fig. 4B).

To evaluate the effects of HDACi-induced CD5L production, we performed flow cytometric analysis. HDACi stimulation favored the increase of classical monocytes ($p = 0.063$), having no significant effect on the intermediate and non-classical subsets (Fig. 4C). Also, HDACi increased $\alpha_M$-integrin (CD11b) expression within the CD4⁻CD11b⁺ gate ($p = 0.016$).

Correlation analyses showed that CD5L levels in HDACi-treated cells correlated positively with the proportion of non-classical CD14$^{low}$CD16⁺ monocytes (Spearman $\rho = 0.582$, $p = 0.0009$) and with CD16 expression by MFI on this subset ($\rho = 0.529$, $p = 0.003$), which collectively suggested a connection between non-classical monocyte activation and CD5L production (Fig. 4B). IL-10 production by HDACi-treated cells correlated negatively to CD11b MFI on CD16⁺ monocytes (Fig. 4B), recapitulating the pattern observed following rCD5L stimulation (Fig. 3D). Since rCD5L stimulation increased IL-10 and GAS6 production, these mediators may contribute to the downstream effects of CD5L on PBMCs.

Taken together, these findings support an HDAC-dependent mechanism of CD5L production, acting in conjunction with IL-10 and GAS6 to counteract the accrual of the pro-inflammatory monocyte subset.

### CD5L production delineates the efferocytosis phenotype of CD14⁺ cells

To further characterize the CD5L-producing CD14⁺ cells, we measured CD5L levels in supernatants of LPS-activated CD14⁺ cell cultures of 35 RA patients (Table 1).

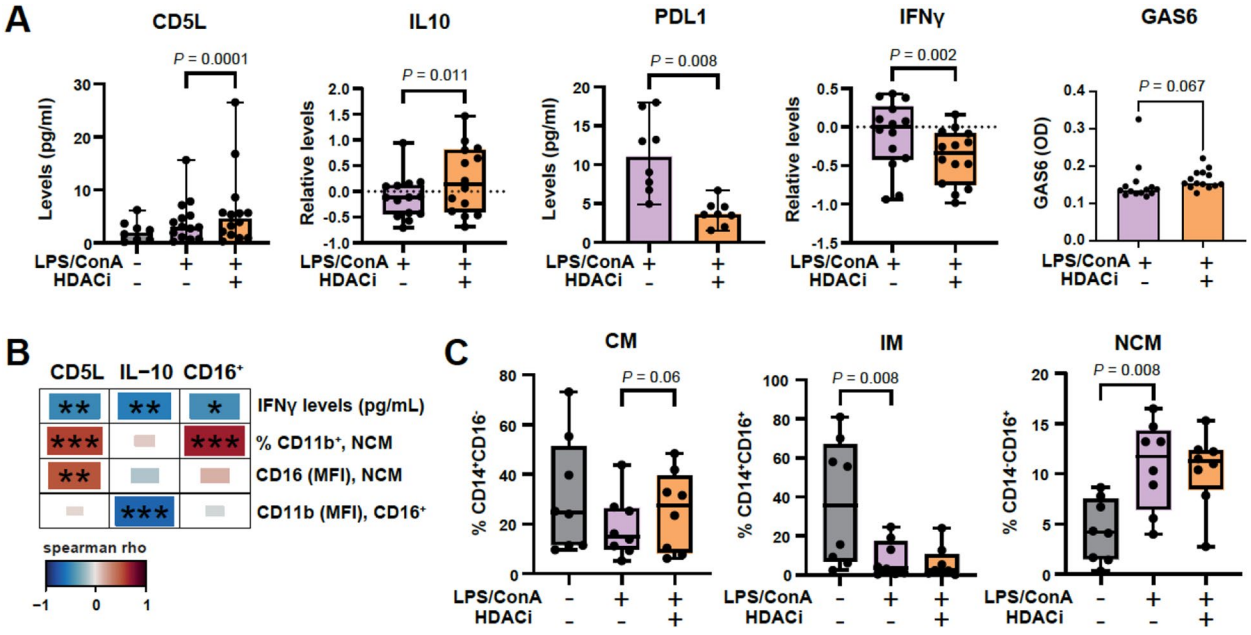


**Fig. 4** HDAC inhibition promotes CD5L production and an anti-inflammatory phenotype in human monocytes. **A** Protein levels in supernatants from human blood leukocyte cultures ($n = 14$) stimulated as indicated. IL-10 and IFN-γ levels were normalized to mock controls. **B** Heat maps showing Spearman correlation coefficients (ρ) between CD5L and IL-10 concentrations in culture supernatants and the frequency of CD16⁺ cells measured by flow cytometry. **C** Frequencies of classical (CM; CD14⁺CD16⁻), intermediate (IM; CD14⁺CD16⁺), and non-classical (NCM; CD14.$^{low}$CD16⁺) monocyte subsets in stimulated human leukocyte cultures ($n = 14$). *p*-values were calculated using the paired Wilcoxon test. * $p < 0.05$; ** $p < 0.01$; *** $p < 0.001$

CD5L protein concentrations exceedingly twice the assay detection limit (0.6 pg/ml) were measurable in the supernatants of 10 out of 35 CD14⁺ cell cultures, hereafter designated as CD5L$^{hi}$CD14⁺ cells. These cells produced significantly higher IL-10 protein levels (27.5 vs. 22 pg/ml, $p = 0.026$) and *IL10* mRNA expression (2262 vs. 133 relative units, $p = 0.0028$) (Fig. 5A, B). Furthermore, RA patients with CD5L$^{hi}$CD14⁺ cells exhibited significantly higher PD-L1 production levels (25.5 vs. 18.87 pg/ml, $p = 0.030$), elevated white blood cell counts (6.85 vs. $5.2 \times 10^9$/l, $p = 0.051$) and platelet counts (293 vs. $225 \times 10^9$/l, $p = 0.0031$), as well as increased serum IFN-γ levels (19.60 vs. 17.02 pg/ml, $p = 0.064$) (Fig. 5A). No differences were observed in the levels of IFN-γ, IL-1β, IL-8, and IL-6 between the supernatants of CD5L$^{hi}$CD14⁺ and CD5$^{low}$CD14⁺ cells (Fig. S5A).

The high IL-10 production by CD5L$^{hi}$CD14⁺ cells was accompanied by transcriptional upregulation of the C1q subunits *C1QA*, *C1QB*, and *C1QC*, which opsonize apoptotic cells and promote efferocytosis (Hulsebus et al. 2016), as well as the TAM receptor *AXL* and pro-resolving regulators *ALOX15B* and *VSIG4*, suggesting that CD5L-producing monocytes acquire an efferocytosis-prone phenotype (Fig. 5B). In agreement with this, the pathway enrichment analysis of the genes functionally dependent on high CD5L production in CD14⁺ cells identified negative regulation of cytokine production and control of immune system processes and cell motility as the top biological processes associated with high CD5L production in CD14⁺ cells (Fig. S5B). Among the suppressed biological processes in CD5L$^{hi}$CD14⁺ cells, the downregulation of ATPase- and GTPase-dependent hydrolase activity was prominently enriched, showing an inverse relationship with CD5L production in CD14⁺ cells.

Taken together, transcriptome analysis of CD5L$^{hi}$CD14⁺ cells revealed the acquisition of an efferocytosis-prone phenotype and enhanced IL-10 production. These findings validated the findings done in HDACi-treated cultures, suggesting that CD5L production by monocytes was reliably associated with suppression of their pro-inflammatory effector functions.

### Serum CD5L levels shape transcriptome of blood CD14⁺ cells

To further explore the effect of extracellular CD5L on RA monocytes in vivo, we analyzed the transcriptome of CD14⁺ cells in relation to serum CD5L levels. Monocyte subset composition was estimated in silico using the normalized sum of RNA-seq expression for subset-specific marker genes identified in a recent single-cell transcriptome study (Binvignat et al. 2024). The IL-1β–rich monocytes exhibited the highest cumulative expression of the subset-specific genes, followed by the classical and IFN-γ-imprinted monocytes, while the non-classical monocytes showed the lowest expression levels compatible with their low frequency (Fig. 6A, B). Among the genes upregulated in proportion with increasing serum CD5L

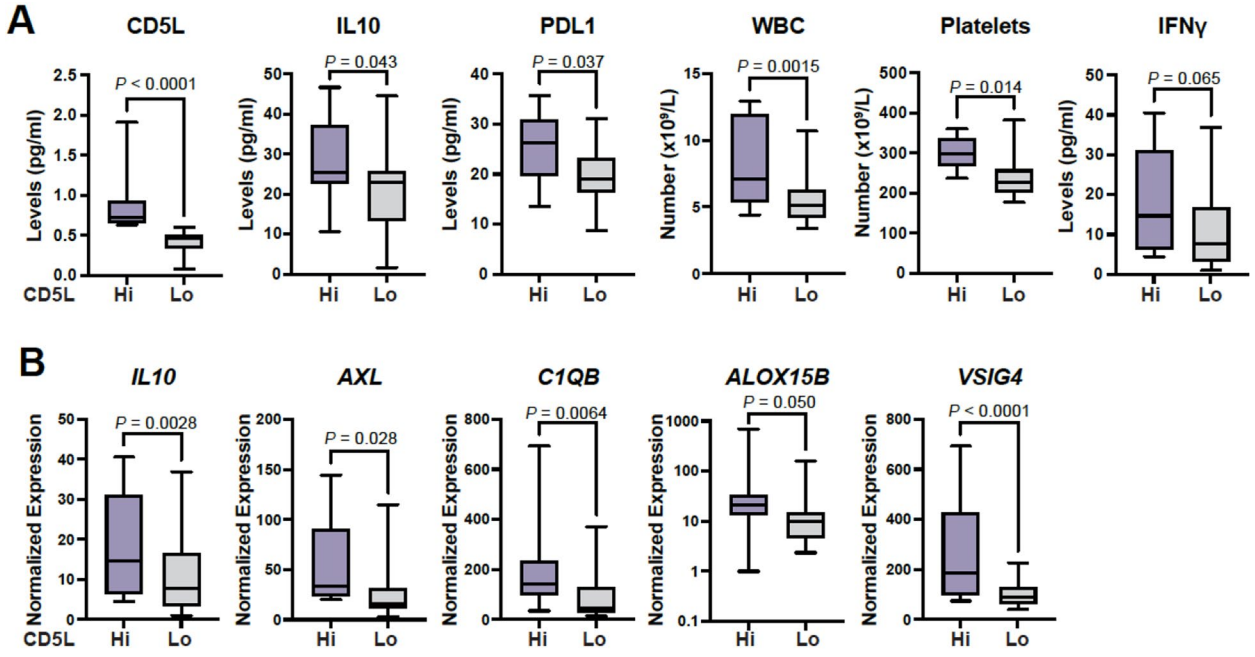


**Fig. 5** CD5L production identifies efferocytosis-prone CD14⁺ monocytes in RA patients. CD5L protein levels were measured in supernatants from CD14⁺ cell cultures of 35 RA patients. Cultures with CD5L concentrations > 0.6 pg/mL (twice the detection limit) were classified as $CD5L^{hi}$ (n = 10), whereas the remaining samples were classified as $CD5L^{low}$ (*n* = 25). **A** CD5L, IL-10, and PD-L1 protein levels in culture supernatants; white blood cell (WBC) and platelet counts; and serum IFN-γ levels in $CD5L^{hi}$ and $CD5L^{low}$ patients. **B** Normalized gene expression in CD14⁺ cells measured by RNA-seq. Differential expression analysis was performed using DESeq2, and nominal *p*-values are indicated

levels, we identified the genes of non-classical monocytes including *FCGR3A*, *MT2A*, *C1QA*, *C1QB*, and *LILRA5* (Fig. 6C, left), which reproduced the experimental findings of CD5L-dependent enrichment for $CD16^+$ monocytes. Additionally, the signature genes of the IFN-imprinted monocytes, including *ISG15*, *TYMP*, *FTH1*, and, also, *IFNG*, *JUN*, *CEBPB* and *CBX6* genes, were upregulated in parallel with increasing serum levels of CD5L (Fig. 6C, right).

Further analysis of the CD14⁺ cell transcriptome in relation to serum CD5L levels revealed the accumulation of genes consistent with the pro-efferocytosis phenotype observed in $CD5L^{hi}CD14^+$ cells. This included increased expression of *C1QB* and *CXCL16*, which opsonize apoptotic cells and PS-coated bodies; transcription factors *MAFB* and *NR4A1*, which govern anti-inflammatory molecules *NFKBID* and *NR4A3* that repress the NF-κB pathway; upregulation of the TAM receptor ligand *GAS6*, mediating *SOCS1* production; and regulators of inflammation resolution such as *ALOX15B* and *FPR2*, potentially enhancing efferocytosis capacity (Fig. 6D).

By contrast, several lysosomal genes involved in the apoptotic cargo processing were downregulated with increasing serum CD5L levels. The later included the RNASE genes, multiple ABC1 lipid exporters, the cholesterol exporter *NPC1*, and the internalization-related *SMPDL3B*, suggesting insufficient or overloaded efferocytosis (Fig. 6D). Supporting the hypothesis of insufficient efferocytosis, serum CD5L levels were associated with upregulation of the immunoregulatory macrophage program, including the genes *HES4*, *IL4I1*, *CKB*, *CDKN1B/CDKN1C*, and *VSIG4* (Fig. 6D), previously identified in tumor-conditioned macrophages (Mulder et al. 2021; Wang et al. 2024), indicating dampened resolution biochemistry and impaired apoptotic cell clearance.

Taken together, these findings demonstrate that serum CD5L levels shape the transcriptome of CD14⁺ cells in RA, promoting the formation of efferocytosis-prone monocytes, while also contributing to the accumulation of non-classical, IFN-primed monocytes with potentially harmful intra-articular effects, as summarized in a CD5L-conditioned monocyte model (Fig. 6E).

### Serum CD5L levels are associated with increased joint skeletal damage in RA

Serum CD5L levels were measured in 80 RA patients and 11 healthy volunteers (Table 1). We found that serum CD5L levels tended to be higher in RA patients than in controls ($p = 0.057$; Fig. 7A, left). Comparing paired samples of serum and synovial fluid of 5 RA patients, we found a significant accumulation of CD5L levels in the joint cavity of RA patients ($p = 0.038$; Fig. 7A, right), consistent with a previous report (Yasuda et al. 2024).

We then assessed the correlation between CD5L serum levels and clinical characteristics of RA patients. This analysis revealed a positive correlation between

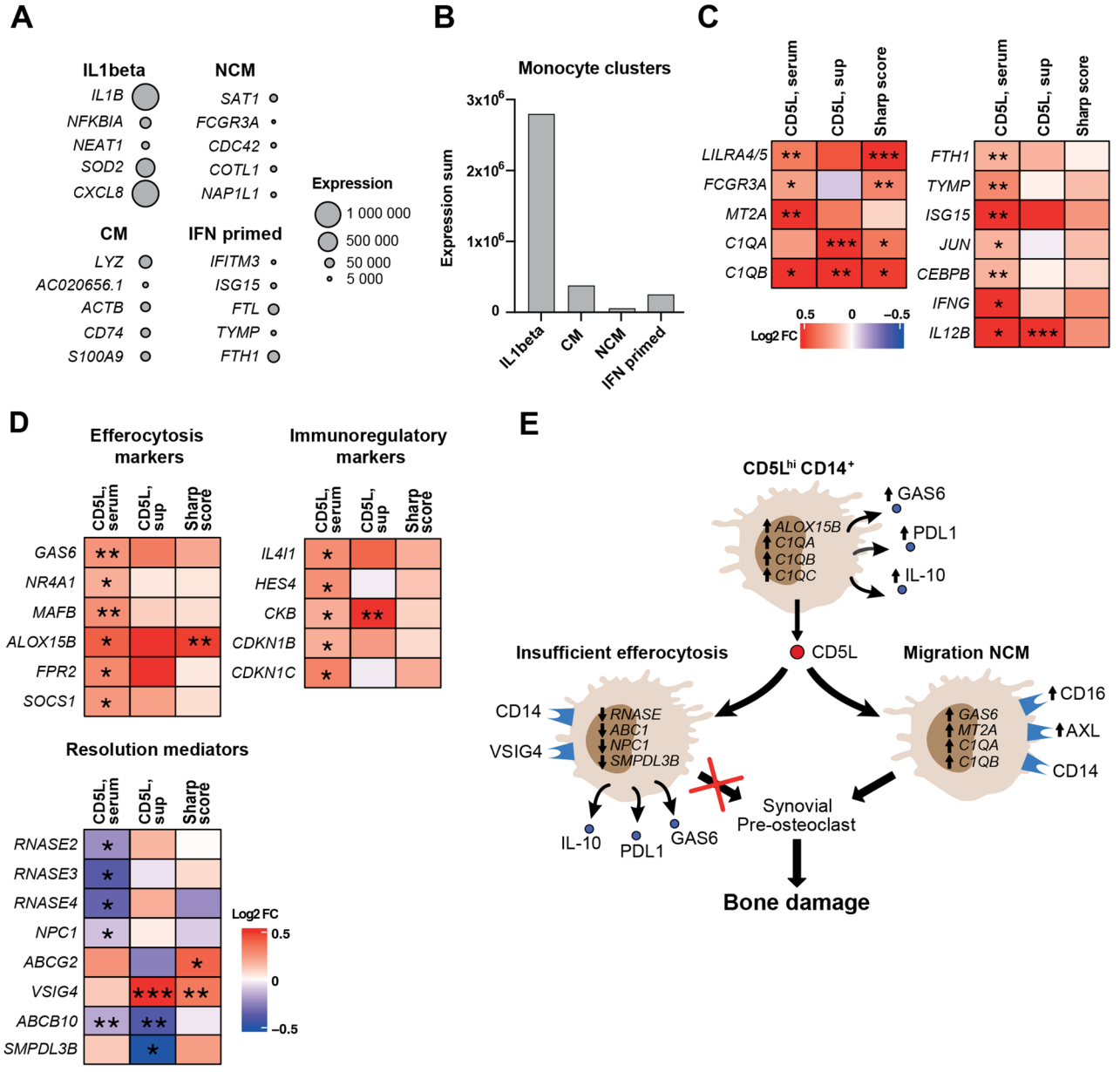


**Fig. 6** CD5L shapes the transcriptional profile of CD14⁺ monocytes in RA patients. **A** Mean normalized expression of gene markers defining IL-1β-enriched, classical (CM), non-classical (NCM), and IFN-primed monocyte clusters in CD14⁺ cells, assessed by RNA-seq. **B** Distribution of monocyte clusters based on the summed expression of cluster-specific marker genes. **C** Gene expression changes ($log_2$ fold change) in non-classical (left) and IFN-primed (right) monocyte clusters in relation to serum CD5L levels and the vdH–Sharp score. Differential expression analysis was performed using DESeq2; nominal *p*-values are indicated. **D** Gene expression changes ($log_2$ fold change) of efferocytosis markers, resolution mediators, and immunoregulatory macrophage-associated genes in relation to serum CD5L levels and the vdH–Sharp score. **E** Schematic representation of CD5L-associated transcriptional changes in monocytes. * $p < 0.05$; ** $p < 0.01$; *** $p < 0.001$

CD5L levels and RA severity, assessed by clinical disease activity (DAS28, ρ = 0.31, $p = 0.006$), and joint skeletal damage (JSD) quantified by vdH-Sharp score (ρ = 0.402, $p = 0.00022$) (Fig. 7B, C). Although, there was also an inverse correlation between CD5L and serum COMP (ρ = –0.30, $p = 0.026$) and CTX-I levels (ρ = –0.32, $p = 0.078$), acknowledged biomarkers of bone and cartilage metabolism (Sakthiswary et al. 2017; Lindqvist et al. 2005).

Linear regression analysis revealed a significant association between serum CD5L levels and vdH-Sharp scores in radiographs of hands and feet (Fig. 7C, left). Analysis of JSD in the 35 RA patients, the source of the CD14⁺ cells used in this study, showed correlations between vdH-Sharp scores and disease duration (Spearman

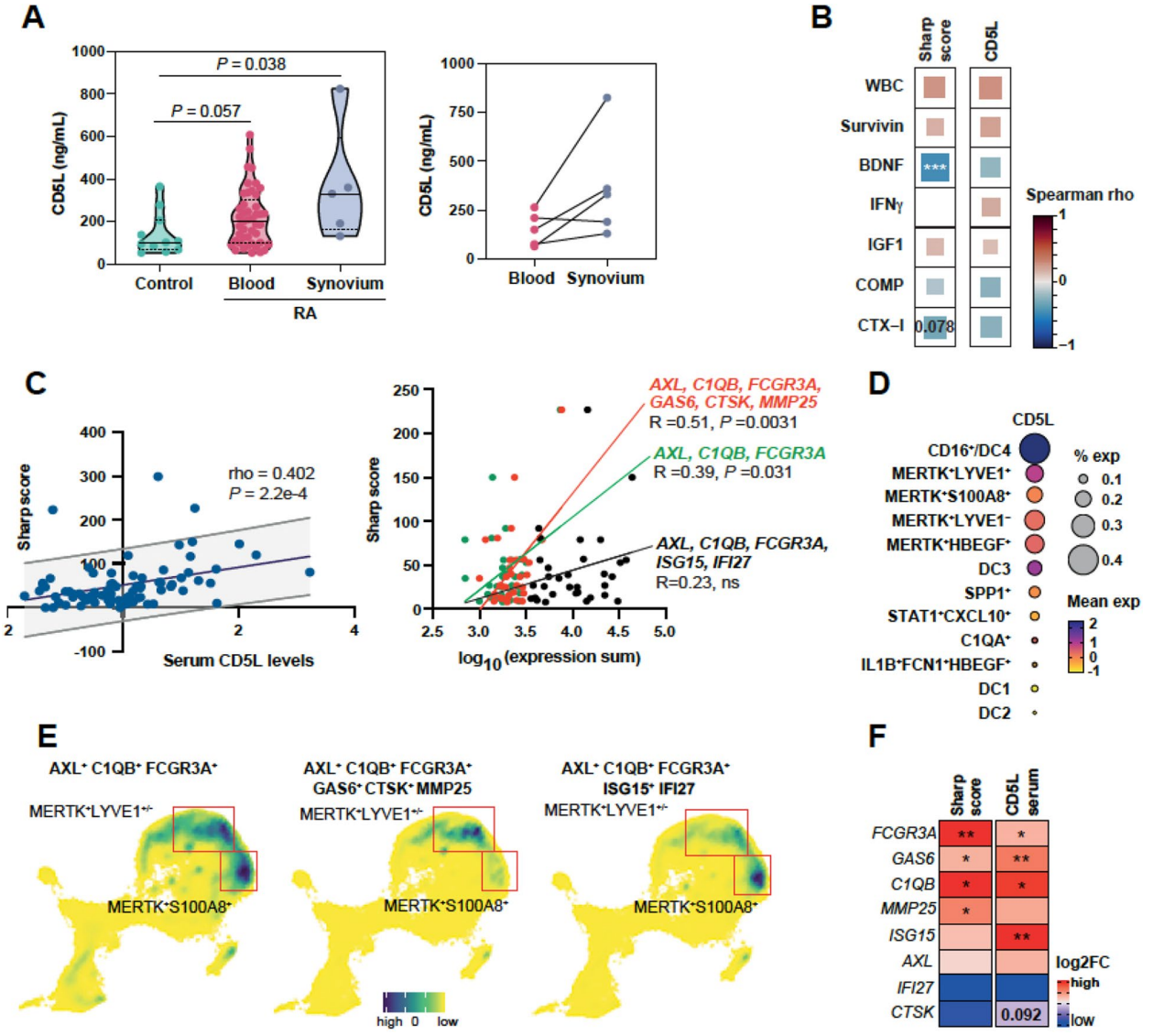


**Fig. 7** Low CD5L expression in synovial macrophages associates with joint damage in RA. **A** CD5L protein levels in serum from RA patients and healthy controls (left), and paired serum and synovial fluid samples from RA patients (right). **B** Spearman correlation coefficients (ρ) between serum CD5L levels or vdH–Sharp score and serological markers. **C** Correlation analyses of serum CD5L levels versus vdH–Sharp score in 80 RA patients (left), and the CD5L-dependent gene signature in non-classical monocytes versus vdH–Sharp score (right). **D** Frequency of CD5L$^+$ cells within the synovial myeloid cell cluster. **E** UMAP visualization of CD5L-dependent signature expression in synovial myeloid cells assessed by single-cell RNA-seq. **F** Gene expression changes ($log_2$ fold change) in the CD5L-dependent osteoclastogenic signature of blood CD14$^+$ cells in relation to vdH–Sharp score and serum CD5L levels. Differential expression analysis was performed using DESeq2; nominal *p*-values are indicated. * $p < 0.05$; ** $p < 0.01$; *** $p < 0.001$

ρ = 0.503, $p = 0.004$), as well as with serum levels of IL-8 (ρ = 0.369, $p = 0.041$), BDNF (ρ = −0.470, $p = 0.008$), and RANKL (ρ = −0.346, $p = 0.057$).

To explore relationship between JSD and CD5L-dependent transcriptome of CD14$^+$ cells, we compared the genes transcription changed in relation to these two parameters. The pathway enrichment analysis identified the genes functional in leukocyte activation, cell adhesion, and cell motility that were significantly upregulated both in proportion to JSD and to serum CD5L levels (Fig. S5C). Namely, in the regression analysis, both serum CD5L levels and the vdH–Sharp score were associated with markers of efferocytosis-prone monocytes, including *C1QB*, *C1QA*, *GAS6*, *ALOX15B*, *VSIG4*, as well as non-classical features including *FCGR3A*, the *C1Q* subunits, and the *LILRB4/5* receptors, but not with genes characteristic of IFN-primed monocytes (Fig. 7C, right).

### Scant CD5L expression in synovial macrophages facilitates joint damage in RA

To assess CD5L-dependent effect in resident monocytes of synovial tissue, we analyzed the myeloid cell

clusters ($n = 76{,}181$ cells) in RA synovia (Zhang et al. 2023). In total, non-zero *CD5L* expression was detected in only 0.17% (129 out of 76,181) of myeloid cells in RA synovia. Of these *CD5L*-expressing cells, 62% (80 out of 129) were within the MerTK$^+$ clusters, specifically the MerTK$^+$S100A8$^+$, MerTK$^+$SELENOP$^+$LYVE1$^-$, and MerTK$^+$SELENOP$^+$LYVE1$^+$ populations, whereas only 0.05% (6 out of 129) corresponded to monocyte-derived CD16$^+$ dendritic cells, known for their high migratory potential (Fig. 7D). This transcriptome pattern suggested that either predominantly CD5L-deficient monocytes traffic into the RA synovium or, alternatively, that *CD5L* expression is downregulated after macrophages enter the synovial tissue. Consequently, the CD5L imprint on synovial macrophages is likely driven by CD5L availability in the serum or synovial fluid rather than by local production within the joint.

In macrophages and dendritic cells, the TAM family of receptor tyrosine kinases are represented by expression of AXL and MerTK. In experimental arthritis, both AXL and MerTK receptors have anti-inflammatory properties acting in the *FCGR3A* rich setting (Gao et al. 2023). In RA synovial tissue, we found that the CD5L-dependent monocyte signature consisting of *AXL-FCGR3A-C1QB* genes was enriched within the CD5L-expressing and, potentially, inflammation resolving MerTK$^+$LYVE1$^+$ cluster (Alivernini et al. 2020) and within the pro-inflammatory and joint damaging MerTK$^+$S100A8$^+$ cluster (Geven et al. 2016) (Fig. 7E). These cells also possessed high expression of the TAM receptor ligand GAS6 which was upregulated in the transcriptome of blood CD14$^+$ cells in direct proportion to JSD quantified by the vdH-Sharp score and to the increasing serum CD5L levels (Fig. 7F). The MerTK$^+$S100A8$^+$ cluster was marked with IFN-sensitive genes ISG15, IFI27 (Fig. 7E). In contrast, expression of GAS6 and NRA41 recognized MerTK$^+$LYVE1$^+$ cluster (Fig. 7E).

To elucidate a connection between *AXL, C1QB,* and *FCGR3A* gene expression and JSD, we analyzed the osteoclast progenitor markers *CTSK*, coding for cathepsin K, and *MMP25* in the defined MerTK$^+$LYVE1$^+$ and MerTK$^+$S100A8$^+$ clusters. We found that CTSK$^+$MMP25$^+$ pro-osteoclasts were enriched within the MerTK$^+$LYVE1$^+$ cluster and combined with *GAS6* gene expression. The expression sum of *AXL, FCGR3A, C1QB, GAS6, CTSK, MMP25* genes in blood CD14$^+$ cells had a strong positive correlation with the vdH-Sharp score of RA patients (Fig. 7C, right). Interestingly, the CD5L-dependent markers of post-engulfing processing and serial efferocytosis *ALOX15B, FPR2/3, RENASE2, VSIG4, NPC1, ABCG1/2, and HES4*, were not expressed in MerTK$^+$ clusters of RA synovia, reflecting the low intensity of tissue efferocytosis.

Overall, this functional analysis confirmed that serum CD5L levels were positively related to JSD caused by RA disease. Scant CD5L-expressing myeloid cells in RA synovia could be a reason for the expansion of AXL$^+$FCGR3A$^+$GAS6$^+$ macrophages, which harbored osteoclast progenitors with established joint damaging properties.

## Discussion

In this study, we demonstrated that the exposure to CD5L and CD5L production in CD14$^+$ cells was associated with an anti-inflammatory profile by inducing production of IL-10 and PD-L1 and lowering surface integrins on monocytes. This had inflammation resolving effect by supporting a shift to monocytes engaged in efferocytosis both in culture and in RA patients. In RA patients, increasing serum CD5L levels were associated with the acquisition of a complete efferocytosis program, characterized by high expression of complement C1q subunits, activation of the GAS6/TAM receptor pathway, and upregulation of the resolution promoting genes *ALOX15B* and *FPR2.* This profile is consistent with the efferocytosis potential of monocytes exposed to, or producing, CD5L.

In parallel with inflammation resolving features, the CD5L-treated leukocyte cultures enrich for FCGR3A/CD16$^+$ monocytes, which in RA patients are associated with accumulation of IFN-primed and non-classical monocytes. The pro-inflammatory program activated by IFN-priming is expected to reduce efferocytosis capacity (Kang et al. 2017). Additionally, development of two other processes in RA monocytes counteracted efficient efferocytosis that were transcriptional depression of resolution/efflux machinery (ABC1 family genes, NPC1, RNASEs) and upregulation of immunoregulatory genes (*HES4*, *IL4i1*, *CKB*, *CDKN1B*/*CDKN1C*, *VSIG4*) leaving a free way for the IFN-primed non-classical monocytes into RA joints.

The bulk transcriptome of CD14$^+$ cells was used in the exploratory part of the study, thus development of anergic or low metabolic monocytes and enrichment for the tissue trafficking monocyte subset could present two parallel and even competing events ongoing in different cells. We addressed this notion by analyzing a vast single-cell data set of RA synovia. The analysis unexpectedly demonstrated a profound CD5L deficiency of synovial myeloid cells. In contrast, the TAM-expressing synovial clusters were heavily enriched with non-classical (FCGR3A$^+$C1QB$^+$AXL$^+$) cells fostering osteoclast precursors. Moreover, a CD5L-dependent signature including expression of *FCGR3A*, *C1QB*, *AXL*, *GAS6*, *MMP25* and *CTSK* in blood monocytes of RA patients correlated strongly with the severity of joint skeletal damage.

The joint damaging properties of non-classical CD16$^+$ monocytes have been linked to their ability of osteoclast differentiation in mouse experimental arthritis models (Misharin et al. 2014; Puchner et al. 2018). We offer a further step in this direction and demonstrated that enrichment with non-classical monocyte subsets harbored features of environment dependent adaptation in response to external signals. Co-expression of GAS6 with TAM receptors signify a characteristic feature of such joint-damaging monocytes. TAM receptors AXL and MerTK are negative regulators of bone healing. AXL inhibition prevents osteoclast differentiation (Tanaka et al. 2021), while GAS6 has a bone destructive role in mice periodontitis (Nassar et al. 2017). Additionally, no sign of osteoclast inclination was found in the IFN-primed FCGR3A$^+$C1QB$^+$AXL$^+$ synovial macrophages consistent with their high motility and adhesion profile described in systemic sclerosis (Villanueva-Martin et al. 2023).

We observed that CD5L increase occurred in the pre-arthritis and early arthritis phases of CIA in WT mice. Whether the rise of serum CD5L is characteristic for pre-clinical phase of RA remains to be explored. No clinical arthritis was registered in WT mice during the period corresponding to CD5L increase. Consistent with previous reports of anti-inflammatory propertied of CD5L (Arai et al. 2016; Maehara et al. 2021), CD5L-deficiency in CIA mice was associated with a remarkable efflux of monocyte/macrophages into the blood (Sanjurjo et al. 2018), and excessive pro-inflammatory environment characterized by an excessive production of IL-1β, IL-17, and IFN-γ, which drive synovitis and joint damage by further attracting myeloid cells (Kuwabara et al. 2017; Palmblad et al. 2001; Srirangan and Choy 2010; Kato 2020). Notably, the increase of proinflammatory cytokines in CD5L$^-$ mice converged with the increase of CD5L in WT mice, which could have dampened the cytokine release offering explanation to why it did not occur in WT mice. Together, the results of animal arthritis model and of human RA material strongly suggest that CD5L does not promote inflammation in RA but rather serves as a protective factor.

In this study, we connected CD5L production with the basic cellular processes in human CD14$^+$ cells. We demonstrated that production of CD5L required inhibition of histone deacetylases, the enzymes with immediate control of gene transcription. CD5L appeared to be specifically dependent on this molecular mechanism, as neither of the pro-inflammatory stimulants, LPS/ConA or FCGR-activating IgG, alone was sufficient to increase CD5L production. Notably, we demonstrated that human leukocytes treated with HDACi downregulated production of IFN-γ, which bound together production of CD5L, IL-10 and accumulation of CD16$^+$ monocyte subsets. In mice, this partnership of histone deacetylases with IFN-γ in regulation of monocyte phenotype has been shown dependent on HDAC3 and significantly affected about 50% of cytokine profile in mouse monocytes (Chen et al. 2012).

Inflammation recruits HDAC to repress macrophage genes (Marques et al. 2025). This could be translated in upregulation of CD5L with HDAC inhibition contrasting with the view on inflammation as a strong HDAC inhibitor at early phase of arthritis. The pathogenic role of histone acetylases in arthritis has been demonstrated in mouse models while HDACi delayed arthritis development and alleviated its severity (Angiolilli et al. 2017; Joosten et al. 2011; Lin et al. 2007; Grabiec et al. 2012), although the studies prioritized the effect of HDACi on synovial fibroblasts rather than macrophages. Our study proposes a CD5L-dependent link between the tissue trafficking of FCGR3A/CD16$^+$ monocytes and development of skeletal damage.

In conclusion, this study demonstrated that the anti-inflammatory and inflammation resolving properties of CD5L are executed through induction of efferocytosis profile in monocytes. In human RA, high serum levels of CD5L harbor a potential danger of uncontrolled invasion of non-classical monocytes into synovial tissue causing structural joint damage. The complex role of CD5L in inflammation and disease outcomes requires careful consideration of disease phase and experimental context.

## Supplementary Information

The online version contains supplementary material available at https://doi.org/10.1186/s10020-026-01456-x.

Supplementary Material 1. Fig. S1 Gating strategy used to identify leukocyte populations in the blood of WT and CD5L$^-$ mice. Cells were identified as T cells (CD3+), B cells (CD19+), NK cells (NK1.1+CD3–), eosinophils (SSChighSiglec-F+CD11b+), neutrophils (Siglec-F–Ly6G+CD11b+), monocytes (Siglec-F–Ly6G–F4/80+CD11b+), classical/inflammatory monocytes (Siglec-F–Ly6G–F4/80+CD11b+Ly6C+), and patrolling/non-classical monocytes (Siglec-F–Ly6G–F4/80+ CD11b+Ly6C–). Fig. S2 Weight and joint histology of WT and CD5L$^-$ mice in the CIA model. Mice were immunized with chicken collagen on day 0 followed by a boost administration of the antigen on day 21. (A) Weigh at baseline (day 0) in WT and CD5L$^-$ mice cohort included in the experiments (left) and weight variation upon arthritis induction (right). Graphical representation of median and 25th – 75th quartiles (left) or mean with SEM (right), n= 36 (WT) and n= 39 (CD5L$^-$) mice per group, pooled from five independent experiments. (B) representative joint tissue sections of WT and CD5L$^-$ mice recovered at day 56 post CIA, stained with hematoxylin and eosin. Bone (B), bone marrow (BM) and joint space (JS) are indicated. Presence of inflammatory infiltrate is indicated by black arrows in the CD5L$^-$ tissue section (right). Fig. S3. Dynamics of leukocyte populations and anti-collagen antibodies in the blood of WT and CD5L$^-$ mice in the CIA model. Mice were immunized with chicken collagen on day 0 and received a booster injection on day 21. (A) Frequencies of the indicated leukocyte populations were analyzed at different time points after immunization in peripheral blood of WT and CD5L$^-$ mice by flow cytometry (expressed as frequencies of total live cells). Phenotypic markers were as follows: T cells (CD3$^+$), B cells (CD19$^+$), neutrophils (Siglec-F$^-$Ly6G$^+$CD11b$^+$), NK cells (NK1.1$^+$CD3$^-$), and eosinophils (SSChighSiglec-F$^+$CD11b$^+$). Data are shown as mean ± SEM for n = 10 WT and n = 10 CD5L$^-$ mice pooled from two independent experiments. Sta-

tistical comparisons were performed using Šídák's multiple-comparisons test. (B) Anti-collagen IgG levels were measured in serum from WT and CD5L$^-$ mice by ELISA at the indicated time points after immunization. Data are presented as median with 25th-75th percentiles. * $p < 0.05$; ** $p < 0.01$. Fig. S4 Modulation of monocyte subsets and CD5L production following pharmacologic stimulation. (A) Representative flow cytometry plots showing the gating strategy for CD11b$^+$CD4$^-$ monocytes. (B) Frequencies of monocyte subtypes within CD11b$^+$CD4$^-$ cells following stimulation with LPS/ConA in the presence or absence of rCD5L or IgG, as indicated. (C) CD5L concentrations in PBMC culture supernatants measured by ELISA. (D) IFN-γ concentrations in PBMC culture supernatants under the indicated conditions. LPS/ConA, lipopolysaccharide/concanavalin A; HDACi, histone deacetylase inhibitor; LynAct, Lyn activator. Fig. S5 Cytokine profile and transcriptomic signatures associated with CD5L-producing CD14$^+$ cells in RA. (A) Cytokine protein levels in supernatants from CD14$^+$ cell cultures of RA patients with high CD5L production (> 0.6 pg/mL, twice the detection limit; n = 10) and low CD5L production (n = 25). (B) Biological processes enriched in the transcriptome of CD5L-producing CD14$^+$ cells, identified by Gene Set Enrichment Analysis (GSEA). (C) Heat map showing gene expression changes ($log_2$ fold change, FC) in relation to serum CD5L levels, CD5L levels in CD14$^+$ cell supernatants, and the vdH–Sharp score. Differential expression analysis was performed using the DESeq2 method. Nominal p-values are indicated as follows: $p < 0.05$; ** $p < 0.01$; *** $p < 0.001$

**Acknowledgements**
We thank the research nurses Anneli Lund and Marie-Louise Andersson at the Rheumatology Clinic, Sahlgrenska University Hospital, for their assistance with blood sampling. We are grateful to all RA patients who participated in this study. We also acknowledge the support of the i3S Translational Cytometry and Animal Facility platforms, as well as Dr. Kristina Forslind for supervision of the radiographic analyses.

**Authors' contributions**
D.B., E.C., M.I.B. and A.M.C. designed the experiments; M.I.B. contributed with patient material; D.B., D.S., M.C.E., E.C., M.C.S., R.F.S and L.O. performed the experiments; D.B., D.S., M.C.E., V.C., E.C., L.O., M.I.B. and A.M.C. analyzed biological data; V.L. analyzed radiographic material; D.B., D.S., M.C.E., V.C., and L.O. generated the figures; D.B., M.I.B., D.S., V.C., and A.M.C. wrote the paper; D.B., L.O., M.I.B. and A.M.C. reviewed and edited the paper. All authors read and approved the manuscript.

**Funding**
This work was funded by National Funds through FCT—Fundação para a Ciência e a Tecnologia, I.P., under the project UID/4293/2025, and by grants from the Swedish Association against Rheumatism (MB, R-860371, R-994505, R-1013204), the King Gustaf V:s 80-year Foundation (MB, FAI-2020–0653, FAI-2022–0882), the Regional agreement on medical training and clinical research in the Western Götaland county (MB, ALFGBG-965623, ALFGBG-1006725), the University of Gothenburg. The funding sources have no role in study design; in the collection, analysis, and interpretation of data; in the writing of the report; and in the decision to submit the paper for publication.

**Data availability**
Transcriptome sequencing data of CD14 + cells from 35 RA patients is deposited in NCBI GEO with accession GSE282517. Single-cell transcriptomic data of RA synovial tissue are publicly available on Synapse (https://doi.org/10.7303/syn52297840).

## Declarations

**Competing interests**
The authors declare no competing interests.

**Author details**
[1]i3S - Instituto de Investigação E Inovação Em Saúde, Universidade Do Porto, Porto, Portugal
[2]IBMC - Instituto de Biologia Molecular E Celular, Porto, Portugal
[3]Department of Rheumatology and Inflammation Research, Institute of Medicine, Sahlgrenska Academy, University of Gothenburg, Gothenburg, Sweden
[4]Rheumatology Clinic, Sahlgrenska University Hospital, Gothenburg, Sweden
[5]ESS, Politécnico Do Porto, Porto, Portugal

Received: 5 January 2026 / Accepted: 5 March 2026
Published online: 24 March 2026

**References**

Aletaha D, Smolen J, Ward MM. Measuring function in rheumatoid arthritis: identifying reversible and irreversible components. Arthritis Rheum. 2006;54(9):2784–92.
Alivernini S, et al. Distinct synovial tissue macrophage subsets regulate inflammation and remission in rheumatoid arthritis. Nat Med. 2020;26(8):1295–306.
Almutairi KB, et al. The Prevalence of Rheumatoid Arthritis: A Systematic Review of Population-based Studies. J Rheumatol. 2021;48(5):669–76.
Angiolilli C, et al. Histone deacetylase 3 regulates the inflammatory gene expression programme of rheumatoid arthritis fibroblast-like synoviocytes. Ann Rheum Dis. 2017;76(1):277–85.
Arai S, et al. Apoptosis inhibitor of macrophage protein enhances intraluminal debris clearance and ameliorates acute kidney injury in mice. Nat Med. 2016;22(2):183–93.
Binvignat M, et al. Single-cell RNA-Seq analysis reveals cell subsets and gene signatures associated with rheumatoid arthritis disease activity. JCI Insight. 2024;9(16):e178499.
Blanco-Carmona, E., Generating publication ready visualizations for Single Cell transcriptomics using SCpubr. bioRxiv, 2022: p. 2022.02.28.482303.
Cai B, et al. MerTK signaling in macrophages promotes the synthesis of inflammation resolution mediators by suppressing CaMKII activity. Sci Signal. 2018;11(549):eaar3721.
Cardoso MS, et al. CD5L is upregulated upon infection with *Mycobacterium tuberculosis* with no effect on disease progression. Immunology. 2024;173(2):310–20.
Chen X, et al. Requirement for the histone deacetylase Hdac3 for the inflammatory gene expression program in macrophages. Proc Natl Acad Sci U S A. 2012;109(42):E2865–74.
Culemann S, et al. Locally renewing resident synovial macrophages provide a protective barrier for the joint. Nature. 2019;572(7771):670–5.
Faas M, et al. IL-33-induced metabolic reprogramming controls the differentiation of alternatively activated macrophages and the resolution of inflammation. Immunity. 2021;54(11):2531-2546 e5.
Gangadharan B, et al. Novel serum biomarker candidates for liver fibrosis in hepatitis C patients. Clin Chem. 2007;53(10):1792–9.
Gao L, et al. Receptor tyrosine kinases Tyro3, Axl, and Mertk differentially contribute to antibody-induced arthritis. Cell Commun Signal. 2023;21(1):195.
Gebe JA, et al. Molecular cloning, mapping to human chromosome 1 q21-q23, and cell binding characteristics of Spalpha, a new member of the scavenger receptor cysteine-rich (SRCR) family of proteins. J Biol Chem. 1997;272(10):6151–8.
Geven EJ, et al. S100A8/A9, a potent serum and molecular imaging biomarker for synovial inflammation and joint destruction in seronegative experimental arthritis. Arthritis Res Ther. 2016;18(1):247.
Grabiec AM, et al. Histone deacetylase inhibitors suppress rheumatoid arthritis fibroblast-like synoviocyte and macrophage IL-6 production by accelerating mRNA decay. Ann Rheum Dis. 2012;71(3):424–31.
Gravallese EM, Firestein GS. Rheumatoid Arthritis - Common Origins, Divergent Mechanisms. N Engl J Med. 2023;388(6):529–42.
Guo Y, Zhu M, Shen R. CD5L deficiency protects mice against Bleomycin-Induced Pulmonary Fibrosis. Front Biosci-Landmark. 2023;28(9):209.
Hulsebus HJ, et al. Complement component C1q programs a pro-efferocytic phenotype while limiting TNFalpha production in primary mouse and human macrophages. Front Immunol. 2016;7:230.
Isaacs JD. The changing face of rheumatoid arthritis: sustained remission for all? Nat Rev Immunol. 2010;10(8):605–11.
Joosten LA, et al. Inhibition of HDAC activity by ITF2357 ameliorates joint inflammation and prevents cartilage and bone destruction in experimental arthritis. Mol Med. 2011;17(5–6):391–6.

Kang K, et al. Interferon-gamma represses M2 gene expression in human macrophages by disassembling enhancers bound by the transcription factor MAF. Immunity. 2017;47(2):235-250 e4.
Kato M. New insights into IFN-gamma in rheumatoid arthritis: role in the era of JAK inhibitors. Immunol Med. 2020;43(2):72–8.
Kim WK, et al. Glycoproteomic analysis of plasma from patients with atopic dermatitis: CD5L and ApoE as potential biomarkers. Exp Mol Med. 2008;40(6):677–85.
Klein K, Ospelt C, Gay S. Epigenetic contributions in the development of rheumatoid arthritis. Arthritis Res Ther. 2012;14(6):227.
Kuo D, et al. HBEGF(+) macrophages in rheumatoid arthritis induce fibroblast invasiveness. Sci Transl Med. 2019;11(491):eaau8587.
Kurokawa J, et al. Macrophage-derived AIM is endocytosed into adipocytes and decreases lipid droplets via inhibition of fatty acid synthase activity. Cell Metab. 2010;11(6):479–92.
Kuwabara T, et al. The Role of IL-17 and Related Cytokines in Inflammatory Autoimmune Diseases. Mediators Inflamm. 2017;2017:3908061.
Lai X, et al. Elevation of serum CD5L concentration is correlated with disease activity in patients with systemic lupus erythematosus. Int Immunopharmacol. 2018;63:311–6.
Li Y, et al. Reduced activity of HDAC3 and increased acetylation of histones H3 in peripheral blood mononuclear cells of patients with rheumatoid arthritis. J Immunol Res. 2018;2018:7313515.
Li M, et al. CD5L deficiency attenuate acetaminophen-induced liver damage in mice via regulation of JNK and ERK signaling pathway. Cell Death Discov. 2021;7(1):342.
Lin HS, et al. Anti-rheumatic activities of histone deacetylase (HDAC) inhibitors in vivo in collagen-induced arthritis in rodents. Br J Pharmacol. 2007;150(7):862–72.
Lindqvist E, et al. Prognostic laboratory markers of joint damage in rheumatoid arthritis. Ann Rheum Dis. 2005;64(2):196–201.
Maehara N, et al. AIM/CD5L attenuates DAMPs in the injured brain and thereby ameliorates ischemic stroke. Cell Rep. 2021;36(11):109693.
Marques O, et al. Inflammation-driven NF-kappaB signaling represses ferroportin transcription in macrophages via HDAC1 and HDAC3. Blood. 2025;145(8):866–80.
Marsh, S.E., scCustomize: Custom Visualizations & Functions for Streamlined Analyses of Single Cell Sequencing. 2021, GitHub.
Martínez VG, et al. The macrophage soluble receptor AIM/Api6/CD5L displays a broad pathogen recognition spectrum and is involved in early response to microbial aggression. Cell Mol Immunol. 2014;11(4):343–54.
Misharin AV, et al. Nonclassical Ly6C(-) monocytes drive the development of inflammatory arthritis in mice. Cell Rep. 2014;9(2):591–604.
Miyazaki T, et al. Increased susceptibility of thymocytes to apoptosis in mice lacking AIM, a novel murine macrophage-derived soluble factor belonging to the scavenger receptor cysteine-rich domain superfamily. J Exp Med. 1999;189(2):413–22.
Mulder K, et al. Cross-tissue single-cell landscape of human monocytes and macrophages in health and disease. Immunity. 2021;54(8):1883-1900 e5.
Murray PJ, et al. Macrophage activation and polarization: nomenclature and experimental guidelines. Immunity. 2014;41(1):14–20.
Nassar M, et al. GAS6 is a key homeostatic immunological regulator of host-commensal interactions in the oral mucosa. Proc Natl Acad Sci U S A. 2017;114(3):E337–46.
Nogueira E, et al. Enhancing methotrexate tolerance with folate tagged liposomes in arthritic mice. J Biomed Nanotechnol. 2015;11(12):2243–52.
Oliveira L, et al. CD5L as a promising biological therapeutic for treating sepsis. Nat Commun. 2024;15(1):4119.
Palmblad K, et al. Dynamics of early synovial cytokine expression in rodent collagen-induced arthritis : a therapeutic study using a macrophage-deactivating compound. Am J Pathol. 2001;158(2):491–500.
Pincus T, Brooks RH, Callahan LF. A proposed 30-45 minute 4 page standard protocol to evaluate rheumatoid arthritis (SPERA) that includes measures of inflammatory activity, joint damage, and longterm outcomes. J Rheumatol. 1999;26(2):473–80.
Puchner A, et al. Non-classical monocytes as mediators of tissue destruction in arthritis. Ann Rheum Dis. 2018;77(10):1490–7.
Riedel BC, et al. Uncovering biologically coherent peripheral signatures of health and risk for Alzheimer's disease in the aging brain. Front Aging Neurosci. 2018;10:390.
Saeki N, Imai Y. Crosstalk between synovial macrophages and fibroblasts in rheumatoid arthritis. Histol Histopathol. 2023;38(11):1231–8.
Sakthiswary R, et al. Cartilage oligomeric matrix protein (COMP) in rheumatoid arthritis and its correlation with sonographic knee cartilage thickness and disease activity. Clin Rheumatol. 2017;36(12):2683–8.
Salnikova DI, et al. Target role of monocytes as key cells of innate immunity in rheumatoid arthritis. Diseases. 2024;12(5):81.
Sanchez-Moral L, et al. Multifaceted roles of CD5L in infectious and sterile inflammation. Int J Mol Sci. 2021;22(8):4076.
Sanjurjo L, et al. CD5L promotes M2 macrophage polarization through autophagy-mediated upregulation of ID3. Front Immunol. 2018;9:480.
Sarrias MR, et al. Biochemical characterization of recombinant and circulating human Spalpha. Tissue Antigens. 2004;63(4):335–44.
Sarrias MR, et al. A role for human Sp alpha as a pattern recognition receptor. J Biol Chem. 2005;280(42):35391–8.
Srirangan S, Choy EH. The role of interleukin 6 in the pathophysiology of rheumatoid arthritis. Ther Adv Musculoskelet Dis. 2010;2(5):247–56.
Tanaka M, Dykes SS, Siemann DW. Inhibition of the Axl pathway impairs breast and prostate cancer metastasis to the bones and bone remodeling. Clin Exp Metastasis. 2021;38(3):321–35.
van der Heijde DM, et al. Biannual radiographic assessments of hands and feet in a three-year prospective followup of patients with early rheumatoid arthritis. Arthritis Rheum. 1992;35(1):26–34.
Villanueva-Martin G, et al. Non-classical circulating monocytes expressing high levels of microsomal prostaglandin E2 synthase-1 tag an aberrant IFN-response in systemic sclerosis. J Autoimmun. 2023;140:103097.
Wang C, et al. CD5L/AIM regulates lipid biosynthesis and restrains Th17 cell pathogenicity. Cell. 2015;163(6):1413–27.
Wang W, et al. Identification of hypoxic macrophages in glioblastoma with therapeutic potential for vasculature normalization. Cancer Cell. 2024;42(5):815-832 e12.
Wu X, et al. Apoptosis inhibitor of macrophage/CD5L is associated with disease activity in rheumatoid arthritis. Clin Exp Rheumatol. 2021;39(1):58–65.
Yang C, et al. Epigenetic regulation in the pathogenesis of rheumatoid arthritis. Front Immunol. 2022;13:859400.
Yasuda K, et al. AIM/CD5L ameliorates autoimmune arthritis by promoting removal of inflammatory DAMPs at the lesions. J Autoimmun. 2024;142:103149.
Yu HR, et al. A unique plasma proteomic profiling with imbalanced fibrinogen cascade in patients with Kawasaki disease. Pediatr Allergy Immunol. 2009;20(7):699–707.
Zhang F, et al. Deconstruction of rheumatoid arthritis synovium defines inflammatory subtypes. Nature. 2023;623(7987):616–24.

## Publisher's Note